

THE ROLE OF MICROSTREAMING IN
ULTRASOUND-ENHANCED THROMBOLYSIS

BY

ZACHARY T. HAFEZ

B.S., University of Illinois at Urbana-Champaign, 2006

THESIS

Submitted in partial fulfillment of the requirements
for the degree of Master of Science in Bioengineering
in the Graduate College of the
University of Illinois at Urbana-Champaign, 2008

Urbana, Illinois

Adviser:

Professor William D. O'Brien Jr.

ACKNOWLEDGEMENTS

I would like to express my sincere gratitude to my adviser, Dr. William O'Brien Jr., who through his committed support has shown me how to be a better researcher and how to apply my knowledge beyond the scope of academics.

I would also like to thank Dr. Raymond Fish, who has offered his knowledge and expertise throughout my research. I must offer my gracious thanks for the hard work and dedication of Michael Kurowski and Peter Ling, without whom I would not have been able to complete this research. I would also like to acknowledge and thank Alex Haak, Roberto Lavarello, Dr. Rita Miller, and all of the members of the Bioacoustics Research Laboratory who have supported me and helped me through the years. I would like to thank Scott Sprague from the Electrical Engineering Machine Shop for helping design and build the necessary equipment for my experiments. I must also acknowledge the gracious support of Pat Kovar and his generously patient staff at the Community Blood Services of Illinois for supplying me the biological materials to complete my research. Finally, I would like to thank my family for their support, love, and guidance; through their blessings, and God's, I am able to write this thesis.

This material is based on work supported by National Institutes of Health under Grant No. R37EB02641. Any opinions, findings, and conclusions or recommendations expressed in this material are those of the authors and do not necessarily reflect the views of the National Institutes of Health.

TABLE OF CONTENTS

CHAPTER 1: PURPOSE OF THESIS.....	1
CHAPTER 2: INTRODUCTION TO ULTRASOUND.....	2
2.1 BEGINNINGS OF BIOLOGICAL ULTRASOUND.....	2
2.2 BASIC ULTRASOUND PRINCIPLES	3
2.3 GENERATION OF ULTRASOUND	4
CHAPTER 3: THE COAGULATION CASCADE	8
3.1 THE GENERAL COAGULATION CASCADE.....	8
3.1.1 Initiation in Response to Vascular Injury	8
3.1.2 Full Clot Formation	9
3.2 THE EXTRINSIC PATHWAY.....	10
3.3 THE INTRINSIC PATHWAY.....	11
3.4 THE COMMON PATHWAY	12
3.5 VASCULAR OCCLUSIONS	13
3.5.1 Arterial Clots.....	14
3.5.2 Venous Clots.....	14
3.5.3 Stroke.....	15
3.5.4 Clinical Treatment	16
3.5.5 Clot Age Related to Thrombolysis.....	16
CHAPTER 4: ULTRASOUND CONTRAST AGENTS IN IMAGING AND THERAPEUTIC ULTRASOUND	18
4.1 ULTRASOUND CONTRAST AGENTS	18
4.2 STRUCTURE AND RESPONSE OF ULTRASOUND CONTRAST AGENTS.....	18
4.2.1 Structure of Ultrasound Contrast Agents	19
CHAPTER 5: THERAPEUTIC ULTRASOUND AND ENHANCED THROMBOLYSIS	22
5.1 THERAPEUTIC ULTRASOUND	22
5.2 MICROSTREAMING.....	23
CHAPTER 6: MATERIALS.....	26
6.1 EXPERIMENTAL TANK	26
6.2 POWER SOURCE.....	26
6.3 HYDROPHONE.....	26
6.4 HEATING CONTROLLER	27
6.5 TRANSDUCERS.....	28
6.6 BLOOD.....	29
6.7 ULTRASOUND CONTRAST AGENT	30

CHAPTER 7: METHODS	32
7.1 TRANSDUCER CALIBRATION AND CHARACTERIZATION PROCEDURE	32
7.1.1 Center Frequency Measurement	32
7.1.2 Calibration Procedure	33
7.1.3 Characterization Procedure	34
7.2 BLOOD CLOT PREPARATION	36
7.3 DEFINITY® PREPARATION	38
7.4 EXPERIMENTAL PROCEDURE	39
7.5 STATISTICAL ANALYSIS AND MASS LOSS RELATIVE TO MATCHED CONTROL	41
7.6 THEORETICAL BUBBLE DISPLACEMENT AND VISCOUS SHEAR STRESS CALCULATIONS	44
CHAPTER 8: RESULTS	47
8.1 TABLES OF RESULTS	47
8.2 AVERAGE RELATIVE MASS LOSS FOR VARIOUS PRESSURES	50
8.2.1 Analysis of Pressure Dependence of Average Relative Mass Loss	52
8.3 AVERAGE RELATIVE MASS LOSS FOR VARYING FREQUENCIES	53
8.3.1 Analysis of Average Relative Mass Loss for Varying Frequencies	58
8.4 BUBBLE DISPLACEMENT AMPLITUDE AND OSCILLATORY VISCOUS SHEAR STRESS	59
8.5 AVERAGE RELATIVE MASS LOSS WITH RESPECT TO BUBBLE DISPLACEMENT AMPLITUDE	60
8.6 FREQUENCY DEPENDENCE OF SIMULATED OSCILLATORY BUBBLE DISPLACEMENT ON AVERAGE RELATIVE MASS LOSS	62
CHAPTER 9: DISCUSSION	67
9.1 DISPLACEMENT AMPLITUDE, SHEAR STRESSES, AND MICROSTREAMING	67
9.2 RESONANCE	71
CHAPTER 10: CONCLUSIONS	73
REFERENCES	74
APPENDIX A	79
APPENDIX B	81

To my family

CHAPTER 1: PURPOSE OF THESIS

The purpose of this thesis is to examine how the mechanism of microstreaming affects ultrasound-enhanced thrombolysis. These small gas bodies, when oscillating, displace small amounts of the media surrounding them, creating rapidly moving streams around the surfaces. These small, rapidly moving streams are termed microstreams. It has been proposed that the main contributor to the thrombolytic effect of ultrasound lies in the shear stresses that oscillations of gas bubbles create.

This thesis uses Definity®, a lipid-based ultrasound contrast agent, in an attempt to exaggerate the effects of microstreaming and to provide definitive evidence that microstreaming is, in fact, responsible for ultrasound thrombolysis. It should be noted that the terms “microbubble” and “contrast agent” will be used interchangeably.

This thesis begins with a brief introduction of ultrasound and its history leading up to today’s uses, both for therapeutic and imaging purposes, followed by an explanation of what a thrombus is, how it is formed, and why thrombi can be dangerous if left untreated. Finally, the results of this research are presented and conclusions drawn based on what the data suggest.

Combined with existing research in this area, a new approach to treating vascular thrombosis may be developed and utilized for clinical applications. The importance of having such knowledge, along with the possibility that it may positively affect a person’s health, is a strong motivating factor for this thesis and for continuing research.

CHAPTER 2: INTRODUCTION TO ULTRASOUND

2.1 Beginnings of Biological Ultrasound

The idea of emitting a sound wave in a medium and observing its echo was first explored in the early 1800s by Jean-Daniel Colladon, who used an underwater bell to determine the speed of sound in water (O'Brien 2007). The fundamental physics of sound, waves, and their propagation were more fully realized after the publication of Lord Rayleigh's, *The Theory of Sound* in 1877 (Rayleigh 1945). Though Rayleigh's paper was not the first to describe sound as a wave—that was done by Sir Isaac Newton in his 1687 *Principia Mathematica* (Newton 1678)—it was the first to describe sound waves with a mathematical equation and established the basis of future studies in “modern” acoustics and an understanding of sound wave patterns and transmission. In the later 1800s and early 1900s, studies in sound and reflection began to be deeply investigated. The ability to generate ultrasonic pulses based on physical and mechanical stressing was discovered by Pierre Curie and his brother, Jacques Curie, in 1880. Their ability to apply an electric potential across a quartz crystal and observe a mechanical pressure wave formed the basis for future reception of high-frequency ultrasound (Cobbold et al. 2007).

During the early 1900s, a French scientist, Paul Langévin, invented the use of underwater sound, called sonar, for submarine detection and navigation (O'Brien 2007). His technique, which utilized the piezoelectric studies of the Curie brothers, was perhaps the first use of low-frequency (50 to 200 kHz) ultrasound for underwater object detection. His invention of the quartz-sandwiched transducer was a milestone for

modern ultrasound devices, and subsequently, the first time that its potentially damaging effects to biological tissue were recorded. He reported that “fish placed in the beam in the neighborhood of the source operation in a small tank were killed immediately, and certain observers experienced a painful sensation on plunging the hand in this region” (Langévin 1920). His research is thought by many to have laid the groundwork for the study of the bioeffects of ultrasound.

2.2 Basic Ultrasound Principles

Ultrasound can be defined as mechanical sound pressure waves with frequencies above 20 kHz (Cobbold et al. 2007). The audible range for humans is generally considered in the range of sound frequencies between 20 Hz and 20 kHz, below the ultrasonic range. Figure 2.1 outlines the general sound spectrum with its frequency-dependent ranges. The therapeutic frequencies for ultrasound are considered between 20 kHz and 1 MHz, while frequencies for ultrasound diagnostic imaging are generally greater than 1 MHz.

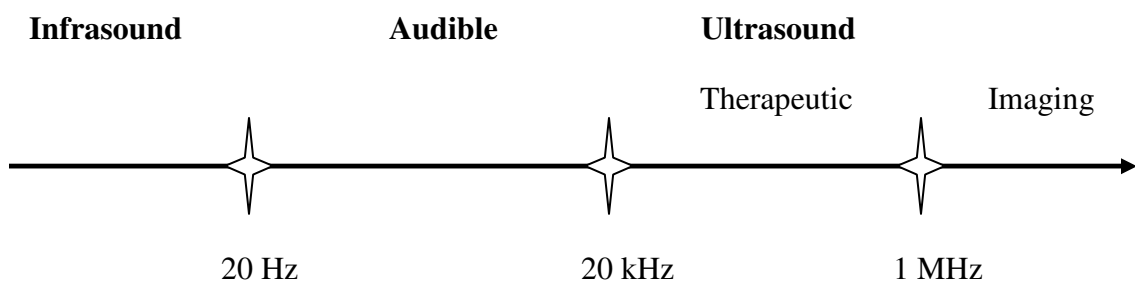


Figure 2.1. Sound spectrum.

Modern-day generation of ultrasound pressure waves utilizes concepts to those used by Langévin in the early 1900s. The discovery by Pierre Curie and Jacques Curie

in 1880 has since been exploited and extrapolated to develop high-frequency sources, linear arrays, and single-element sources, as well as other highly advanced ultrasound devices.

Piezoelectric crystals are grown under conditions that allow them to achieve a certain resonant frequency, referred to as the center frequency of the transducer. Under the application of an electric field, the crystal properties change, resulting in the crystal structure contracting or expanding (Cobbold et al. 2007). What is referred to as “the inverse piezoelectric effect” was predicted and observed by Lippman in the 1880s following the Curie brothers’ discovery. Having grown crystals in desired patterns, researchers have been able to generate simple source elements that emit pressure waves at frequencies specified by the growth of the crystals. This application of piezoelectricity is the modern basis for ultrasound devices and continues to improve as newer materials are discovered and as more-efficient fabrication processes are developed.

2.3 Generation of Ultrasound

The generation of an ultrasound wave begins with an electrical signal sent by a signal generator to the electrical connection of the transducer. This electrical pulse excites the piezoelectric material within the transducer, which causes it to contract or expand, depending on the sign of the pulse. Sinusoidal pulses with positive and negative electrical signals cause the piezoelectric material to expand and contract at the frequency of the sinusoidal input, usually the resonant frequency of the material, which allows the material itself to most efficiently oscillate and thus give maximum amplitude. As the electrically stimulated material expands and contracts, the surface of

the transducer pushes out or in, causing a disturbance in the media that it is exposed to. In the case of sound speakers, which are exposed to air, the diaphragm moves air at specific frequencies, which reaches the ears and is perceived as specific sound. In water, the effect is the same; however, instead of moving air, the piezoelectric material moves sound pressure waves through water. At the fundamental level, particles move at the frequency of the source. The mass movement of particles is enough to create a propagating pressure wave.

The pressure wave can be classified into one of two different categories, depending on its particle motion and the material properties in which it is traveling. Longitudinal waves have particles that move back and forth relative to the direction of propagation and travel in all types of materials, such as gases, liquids, and solids. This is in contrast to shear waves, which have particles that move at right angles with respect to the direction of the propagating wave and travel only through solid media and not found in fluids (O'Brien 2007). Figure 2.2 shows a schematic representation of the two different types of waves that can be generated from a sinusoidal input.

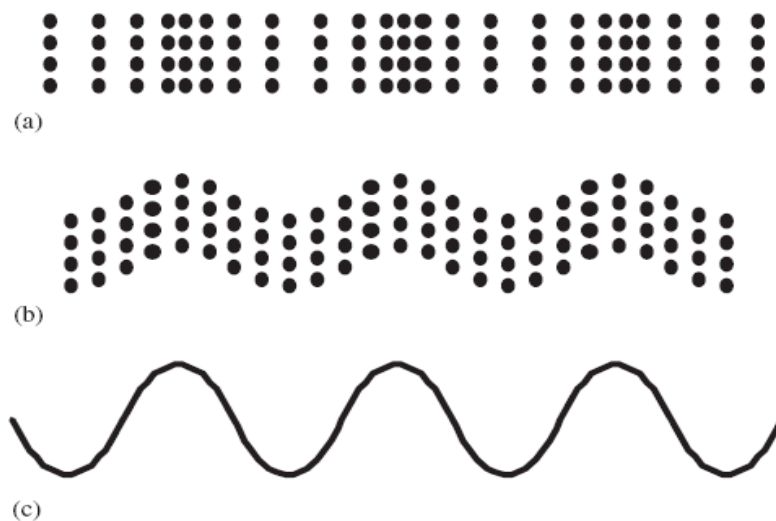


Figure 2.2. (a) Longitudinal wave, (b) shear wave, (c) sinusoidal input (O'Brien, 2007).

Within medical ultrasound, two types of modes are used to generate ultrasonic waves. The continuous excitation of the transducer at constant amplitude creates a continuous wave at the source frequency (O'Brien 2007). This wave, termed a continuous wave, or CW wave, has the ability to deliver large amounts of energy but at low axial resolution for imaging purposes. The other generation mode is to send signals in a pulsed manner. This wave, termed pulsed wave ultrasound, or PW, is more often used in imaging; it has lower intensity but much better axial resolution. Certain parameters can also be changed with pulsed ultrasound, such as the number of cycles per pulse, the amount of time that the pulse is on (its pulse duration), and the fractional amount of time that the pulse is active (duty factor). The relationship of the pulse duration, τ , to the number of cycles, N , and its frequency is given by Equation 2.1 (O'Brien 2007):

$$\tau = NT = \frac{N}{f}. \quad (2.1)$$

Figure 2.3 shows the differences between a continuous wave and a pulsed wave at an operating frequency, f . A single-cycle pulsed wave has a single maximum amplitude peak and single minimum amplitude peak. A continuous wave contains an infinite number of maximum and minimum amplitude peaks; a continuous wave is simply an infinite-cycle pulsed wave. As seen in Figure 2.3, the continuous wave maintains constant amplitude over time, only changing its sign from positive to negative with respective peaks and troughs. The positive pressure amplitude, also called the peak compressional pressure, P_c , and the negative pressure amplitude, also called the peak rarefactional pressure, P_r , are the same value, provided the propagation is under linear conditions. This is contrast to the pulsed wave, where the P_c and the P_r are different in

amplitude as a result of natural dampening affects. The time it takes for the crystals to stop vibrating after they've been excited is known as "ring down" (O'Brien 2007).

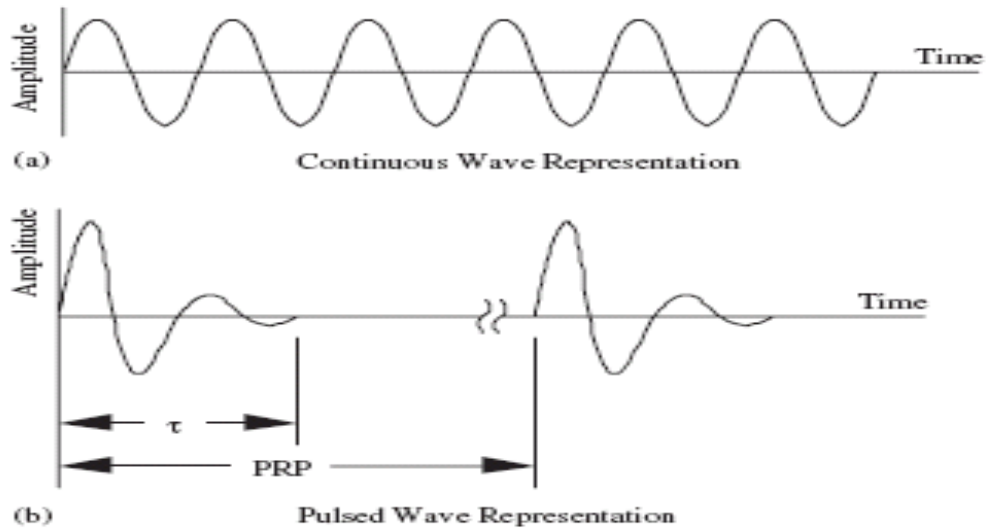


Figure 2.3. Visual representation of a continuous wave (a), and a pulsed wave (b) in time (O'Brien 2007).

CHAPTER 3: THE COAGULATION CASCADE

When a wound is severe enough to sever blood vessels and damage epidermal or connective tissues within the extracellular matrix, the first response, hemostasis prevents further bleeding and limits infection by sealing the wound by way of a complex mechanism that leads to the formation of a blood clot. The mechanism behind blood clotting has been studied in depth and is well understood.

3.1 The General Coagulation Cascade

Blood coagulation, which leads to the formation of a fibrin clot, has two classification pathways, the extrinsic and intrinsic pathways. The *extrinsic pathway* is defined as a pathway initiated when tissue factor, a substance not found within the circulating blood, enters the system. Tissue factor most often includes phospholipids that provide a surface for interaction of various clotting factors. The other pathway, the *intrinsic pathway*, contains all the factors necessary for clot formation within the circulating blood, meaning that nothing extra is needed to initiate the pathway (Harmening et al. 2002). Both pathways eventually lead to generation of the enzyme thrombin, converting fibrinogen to the final fibrin clot.

3.1.1 Initiation in Response to Vascular Injury

The first step of the general coagulation cascade is the formation of platelet clumps, followed by vasoconstriction, then finally the formation of a fibrin clot. The initiation of the clotting cascade begins with blood perfusion through the wound, which cause the cells in the wall of the injured blood vessel to release adenosine diphosphate, ADP, which in turns causes clumps of platelets to adhere to the site of the injury

(Stocum, 2006). Platelets are small particles without nuclei that bud off from megakaryocyte cells and circulate in the body, playing a major role in the clotting process. Blood is kept from clotting in the absence of vascular injury by inert precursor first-phase clotting factors such as factor V, AC-globulin, factor IX, and PTC. Combined with the presence of natural inhibitory factors such as Hageman inhibitor or natural circulating anticoagulants such as heparin, platelet clumping and clot formation are regulated and minimized (Levi et al. 2004).

3.1.2 Full Clot Formation

After a vascular injury, the wound site releases ADP and platelets begin to aggregate. The platelets then begin to degranulate as a result of their exposure to collagen in the walls of the injured vessels and cause the release of ADP, which, in turn, attracts more platelets. This positive feedback system begins to attract other clotting factors such as arachadonic acid, which eventually plays a role in pain, fever, and the inflammation responses. Other factors such as fibrinogen, thrombospondin, and fibronectin are attracted to the wound site as well. These factors act as ligands for platelet aggregation. When these factors come together, the resulting substance is a gluey adhesive that eventually plugs the defect in the vessel wall, much like a carpenter repairing a hole in a wall (Stocum, 2006).

Vasoconstrictors such as thromboxane A₂ and serotonin are released from injured nerve axons, which limits the amount of blood flow into the wound, thus reducing the amount of total blood loss. The nerves also release substance P, a neuropeptide that causes mast cells in the dermis to degranulate, which releases histamine. Histamine has been shown to increase the permeability of vessel walls (Levi

et al. 2004). This increased permeability allows plasma to leak into the wound area. Blood plasma presence is essential in wound healing because it contains coagulation factors that further induce clot formation (Carmeliet et al. 1997).

Continuing the clotting cascade in the development of a full fibrin clot is Hageman factor VII, which has been proven to undergo contact activation with prekallikrein in the presence of a high molecular-weighted cofactor and a negatively charged surface such as kaolin (Hojima et al. 1984). Hageman factor VIII begins by initiating a cascade of reactions involving clotting factors I through XII with calcium (Ca^{2+}) as an essential cofactor. Tissue factor, which is produced at the end of the clotting cascade, converts prothrombin to its active form, an enzyme called thrombin. Thrombin then catalyzes a conversion of plasma fibrinogen to fibrin, which is considered the major structural protein of the clot (Stocum, 2006).

3.2 The Extrinsic Pathway

The extrinsic pathway involves only factor VII, which is activated to factor VIIa in the presence of calcium and the tissue factor, or factor III, which is released from the injured vessel. These three factors are all that are required to activate factor X to Xa, providing a relatively rapid response to an injury and producing small amounts of thrombin, leading to fibrin formation (Harmening et al. 2002). Figure 3.1 shows the flow diagram of the extrinsic pathway leading to the formation of factor X, which then feeds into the common pathway described later. The extrinsic pathway's relatively simple and rapid response allows the body to limit blood loss by quickly initiating after an injury.

Extrinsic Pathway

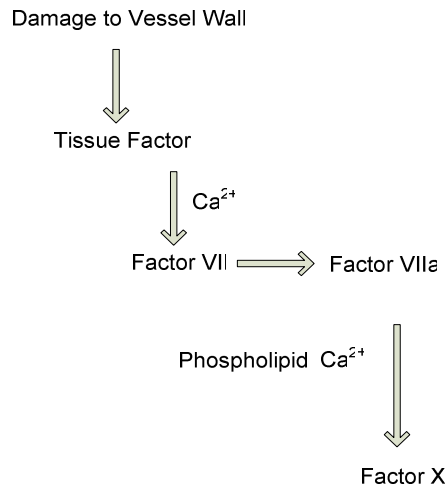


Figure 3.1. The extrinsic clotting pathway.

3.3 The Intrinsic Pathway

The intrinsic pathway is activated following exposure to a negatively charged foreign substance, such as collagen or phospholipids, as previously described.

Following this exposure, activation of factor XII, molecules referred to as contact factors, and factor XI initiate the intrinsic clotting cascade (Harmening et al. 2002).

After it is generated, factor XIIa, in the presence of Fitzgerald factor and Fletcher factor, converts factor XI to XIa. With calcium present, factor IX activates to factor IXa along with cofactors VIII, and platelet factor III activates factor X, leading to the generation of thrombin and the formation of fibrin and a fibrin clot via the common pathway (Stocum, 2006). Figure 3.2 outlines the intrinsic pathway leading to the common pathway. The intrinsic pathway is a more complex cascade than the extrinsic pathway mainly because normal intrinsic injury is not often a life-threatening event;

therefore, it does not need as an immediate and rapid response as the extrinsic pathway does.

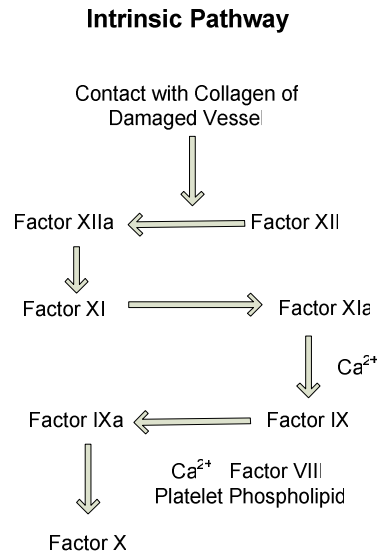


Figure 3.2. The intrinsic clotting pathway.

3.4 The Common Pathway

As previously mentioned, both the intrinsic and extrinsic pathways lead to formation of a fibrin clot. The common pathway begins when factor X is activated by the intrinsic system, the extrinsic system, or by both systems. When factor X is activated, it is converted to Factor Xa in the presence of calcium, phospholipids, and factor V and converts prothrombin to thrombin, its active form (Harmening et al. 2002). Thrombin then, through feedback activation, activates factors VIII and V, converts fibrinogen to a soluble fibrin monomer, and helps to stabilize the fibrin monomer by converting factor XIII to XIIIa (Harmening et al. 2002). The overall coagulation cascade, depicted in Figure 3.3, is a complex, involved process that ultimately leads to

the formation of a solid fibrin mass that stops bleeding and allows the body to begin the second phase of the wound-healing process.

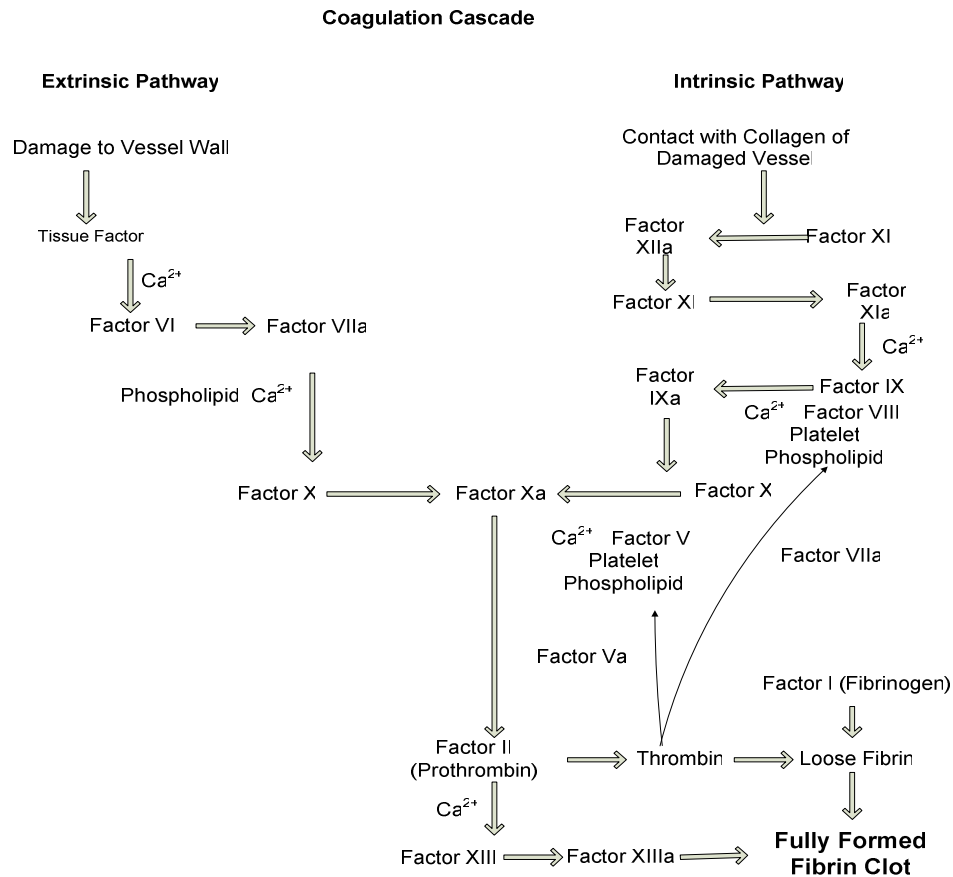


Figure 3.3. The overall coagulation cascade with associated factors and their respective actions.

3.5 Vascular Occlusions

Vascular thrombi can occur as a result of both traumatic and non-traumatic events. Serious complications sometimes occur when a thrombus releases emboli that lodge in arteries that supply blood to organs such as the brain or heart. Occlusion of blood vessels results in reduction of blood flow to the affected area. With any instance of complete or partial ischemia, the resupply of blood flow to the affected tissues is a time-sensitive process—the longer the time that biological tissue is deprived of oxygen, the less chance it will survive or function properly.

3.5.1 Arterial Clots

The formation of arterial clots often stems from the underlying condition of atherosclerosis, which is a condition associated with the build-up of fatty deposits within the arteries. These fatty deposits create turbulent blood flow within the arterial walls (Harmening et al. 2002). Turbulent blood flow causes the clumping of platelets, which initiates the clotting cascade described earlier. Arterial clots may become lodged in coronary arteries, causing complications in the heart, the brain, or the extremities. Clinically, the use of 40 kHz ultrasound has been shown to increase the thrombolysis of coronary arterial clots (Rosenschein et al. 2001). This method of treatment is non-invasive and has been shown to be effective in reducing the size of the blockage as well as reestablishing blood flow to affected areas more rapidly than conventional treatment of blood thinners by disrupting the fibrin matrix of the developed clot (Rosenschein et al. 1997).

3.5.2 Venous Clots

Venous blood clots often form in areas where blood flow is slow, usually in the legs, and often form as a result of factors known as Virchow's Triad: altered blood flow (slow or turbulent), vascular endothelial damage, and hypercoagulability of blood (Yano et al. 2008). The slow-moving blood flow causes pooling of blood in the legs and leads to deep vein thrombi, DVT. Emboli can break off from a DVT and travel to the heart, but most emboli will travel to the lungs. Such pulmonary emboli are a major cause of death. If an arterial or ventricular septal defect in the heart exists, emboli from DVTs may enter the systemic arterial circulation. This can result in emboli to the

coronary arteries, brain, and the rest of the body and cause myocardial infarction, stroke, or other serious problems.

The use of ultrasound is being investigated as a useful method to decrease the amount of DVTs in the legs, which could reduce the chances of developing emboli and vascular occlusions (Kline et al. 2008).

3.5.3 Stroke

Effects of oxygen deprivation seen with ischemic blockage to the brain are referred to as a stroke. With a stroke, blood supply to the brain has been partially blocked. In stroke victims, the time to resupply blood flow to the penumbra region of the brain lacking blood flow is the most crucial factor in how a victim will recover. The most debilitating and catastrophic effects of stroke occur if blood flow is not resupplied to the brain before brain tissue begins to die.

The current approved FDA clinical treatment for all ischemic occlusions is to administer a drug, rt-PA (recombinant tissue plasminogen activator) within three hours of the onset of symptoms. Recombinant (artificially produced) t-PA is similar to the naturally occurring endogenous plasminogen activator in humans. In its natural state, t-PA is produced by vascular endothelium (Magnus et al. 2001). In its native amounts, it is harmless to the body and keeps blood from pooling and forming clots. However, when a traumatic event occurs, the body's intrinsic clotting cascade is activated to prevent internal or external hemorrhaging, or bleeding. Ultrasound has been shown to increase the lytic rate of clots exposed to ultrasound and t-PA, although via unknown mechanisms (Holland et al. 2008).

3.5.4 Clinical Treatment

In the case of a large vascular occlusion, a higher amount of t-PA is necessary to dissolve the thrombus and resupply blood flow before cell and tissue death. The current clinical treatment, as published in *The New England Journal of Medicine* (Stroke rt-PA Study Group 1995), is for rt-PA to be administered as three bolus injections, the first at 90% of the total dose, calculated by body weight (0.9 mg rt-PA /kg body weight), followed by two more injections delivering the remaining 10% twenty minutes apart. However, there are major side effects and harmful consequences of administering these classes of drugs. Because it is an intravenous injection, t-PA perfuses throughout the body, sometimes affecting areas by causing minor or major bleeding (Magnus et al. 2001). Owing to the adverse side effects of t-PA treatment, which can include internal hemorrhaging, a safer, more robust method of dissolving blood clots is needed. In many cases, physicians refuse to use t-PA because no strong data support its efficacy.

3.5.5 Clot Age Related to Thrombolysis

Research has shown a relationship between thrombolysis efficacy and blood clot age. In blood clots exposed to t-PA, clots less than one day old produced approximately 5% more blood loss than clots were of 8 to 14 days of age (Holland et al. 2008). The FDA requires that tests be performed to determine whether blood is safe to handle in laboratory experiments. Those tests took approximately 7 days; thus, the samples used in this study were 7 to 12 days old.

Red blood cells are biologically active outside of the body and can persist until they run out of nutrients or until natural decay. Without nutrients, as the clot ages, the surrounding biological components begin to degrade and atrophy. Older blood clots

appear more resistant to lysis because of clot retraction and platelet atrophy over time (Carroll et al. 1981). Blood with lower platelet counts has a prolonged lysis time. Lysis that occurred in these experiments may be less than what would be experienced *in vivo* because of the platelet decrease in clots 7 to 12 days old.

CHAPTER 4: ULTRASOUND CONTRAST AGENTS IN IMAGING AND THERAPEUTIC ULTRASOUND

4.1 Ultrasound Contrast Agents

Since the early 1990s, medical ultrasound imaging has used contrast agents to increase the brightness of blood-containing structures. Before the use of contrast agents, contrast with ultrasound was limited because the reflected signal of blood was 30 to 60 dB less than that of surrounding tissue. Therefore, a means for increasing the scattering of sound and the echogenicity of a reflected signal in biological tissue and blood gave rise to the development and production of contrast agents. Using the mechanical properties of ultrasound and its reflective boundary conditions with materials, gas-filled contrast agents were developed and have been subsequently used for medical imaging purposes as a way to enhance images by providing better contrast and resolution (Hoff et al. 2007).

Through the use of continuous wave (CW) and pulsed wave (PW) ultrasound, clinical medicine has utilized various elemental and physical parameters of ultrasonic transducers to acquire diagnostic and relevant medical information. In recent years, ultrasound has seen an explosion of uses outside of imaging, mainly from the use of ultrasound contrast agents.

4.2 Structure and Response of Ultrasound Contrast Agents

Ultrasound contrast agents can be injected in the bloodstream and are designed to be small enough to pass through all major and minor capillaries of the human body which range from 5 to 10 μm in diameter. When these microbubbles interact with an

ultrasonic source, they will oscillate or resonate, at a specific frequency defined by (Calliada et al. 1998) in Equation 4.1.

$$f_r = \frac{1}{2\pi a} \sqrt{\frac{3\gamma P_o}{\rho}}. \quad (4.1)$$

The resonant frequency, f_r , is proportional to the square root of the ratio of specific heats, γ , and the ambient pressure, P_o , to the density of the gas in the bubble, ρ , and inversely proportional to the radius of the bubble, a .

In addition to the fundamental resonant frequency, there are also multiple subharmonics and possible ultraharmonics emitted by the bubble. These harmonics are often smaller in intensity but are useful in specific types of imaging, such as harmonic imaging. Their ability to be circulated in the blood is useful to determine flow velocities, as with Doppler imaging, or to examine the perfusion of blood within a tissue. as with perfusion imaging.

4.2.1 Structure of Ultrasound Contrast Agents

The physical make-up of an ultrasound contrast agent is rather simplistic in nature but complex in its response to ultrasound excitation. A typical contrast agent, represented in Figure 4.1, is an encapsulated gas sphere with radius a . A biodegradable shell, with a thickness often ten times smaller than the radius of the bubble, surrounds the inert gas, which prevents it from diffusing, thereby allowing it to last within the human body but also changing its resonant frequency (Szabo et al. 2004), as shown in Equation 4.2:

$$f'_r = \sqrt{\left[f_r^2 + \frac{Sp}{4\pi^2 m} \right]}. \quad (4.2)$$

Not only is the resonant frequency affected by the ambient pressure, specific heat, and density, as in the case with unshelled bubbles (Equation 4.1), but the shell stiffness parameter, S_p , and the effective mass of the system, m , play roles in determining the resonant frequency of shelled bubble. The shell itself has material characteristics that can be altered depending on what materials are used and how the bubble is produced. The gas is often of a high-molecular weight, such as octafluoropropane in the case of Definity contrast agents, which were used for this study.

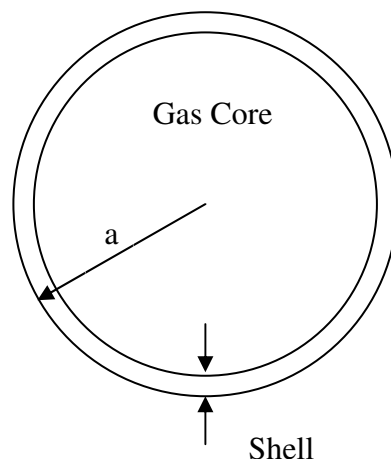


Figure 4.1. Basic ultrasound contrast agent microbubble structure showing inert gas core with shell.

Microbubbles enhance the echo of an ultrasound pulse by exploiting the normal backscattering intensity to acoustic impedance proportionality (Calliada et al. 1998). At the boundary of a microbubble and its surrounding medium, usually blood for diagnostic ultrasound, the impedance difference is large. This large impedance mismatch causes the incident wave to reflect more signal back to the transducer. The reflection coefficient, R , can be determined by Equation 4.3 (Kinsler et al. 2000):

$$|R| = \left| \frac{r_2 - r_1}{r_2 + r_1} \right|. \quad (4.3)$$

It can be seen that if the impedance, r_2 , is much larger compared to the impedance, r_1 , the magnitude of the reflection coefficient is going to be approximately equal to 1, meaning close to 100% of the incident energy, or, in the case of ultrasound, pressure is being reflected. An example is the reflection from a water–air interface, which best mimics the interface of liquid and blood and a gas-filled microbubble. The characteristic impedance of water is $1.48 \times 10^6 \text{ Pa} \cdot \text{s/m}$, and the characteristic impedance of air is $429 \text{ Pa} \cdot \text{s/m}$ (Kinsler et al. 2000). With the impedance value of water being much greater than that of air, close to 99% of the incident pressure is reflected. This principle makes gas-filled microbubbles an optimal choice for ultrasound contrast agents.

CHAPTER 5: THERAPEUTIC ULTRASOUND AND ENHANCED THROMBOLYSIS

5.1 Therapeutic Ultrasound

Paul Langévin's discovery that ultrasound had biological effects has led to research into using ultrasound not only in imaging but also in therapeutic ways. The wide range of uses of ultrasound for therapeutic purposes covers deep tissue heating for massage and healing purposes; sonoporation to allow large molecules to cross cell membranes; angiogenesis to encourage growth of new vasculature within biological tissues for wound healing; tumor ablation to stop the unregulated growth of cells; and thrombolysis, which is proving to be an effective, non-invasive method for dissolving thrombi.

It has been shown that ultrasound in combination with rt-PA can drastically increase the rate at which a blood clot dissolves (Atar et al. 2001; Holland et al. 2008; Stone et al. 2007; Suchkova et al. 2000). However, in each study, the mechanism behind the process remains poorly understood. It has been reported that ultrasound alone does not enhance thrombolysis; rather, it is the combination of rt-PA and ultrasound that gives the maximum lytic effect (Holland et al. 2008).

Many parameters of ultrasound have been investigated, such as pulse length of the ultrasound, the duty factor, and intensity (Cheng et al. 2005; Meunier et al. 2007). It has been shown that an increased pulse length, approaching CW, increases the lytic efficacy of rt-PA with low-frequency (120 kHz) ultrasound, with the proposed mechanisms being acoustic streaming, heating, and increased permeation of the clot to

the surrounding media (Meunier et al. 2007). Furthermore, it has been shown that there may be an intensity dependence, with lower intensities having more of an effect than higher intensities at low-frequency ultrasound, with longer exposure times having increased mass loss (Holland et al. 2008). In addition to thrombolytic drugs, ultrasound contrast agents have been studied as a way to further enhance the effect of ultrasound on the lysis of blood clots *ex vivo*.

5.2 Microstreaming

The theory that led to the belief that microstreaming was responsible for thrombolysis was first developed in 1970, when it was demonstrated that a rigid wire oscillating at low frequencies near human and canine erythrocytes, or red blood cells, released hemoglobin (Williams et al. 1970). Simultaneously in 1970, it was shown that a single pulsating gas bubble at a frequency of 20 kHz released hemoglobin in an erythrocyte suspension (Rooney et al. 1970).

Hemoglobin is a protein that is responsible for the transport of oxygen molecules in red blood cells and is found within the cells. Therefore, it can be released only if red blood cells are lysed or undergo transient sonoporation. The experiments performed by Rooney et al. and Williams et al. demonstrate that the erythrocyte suspensions are being lysed, as evident from the release of heme, which they note in their results.

Furthermore, it has been shown that with an increased number of acoustic microstreaming sources—for example, gas bubbles or microbubbles—there is an increase in the release of hemoglobin and other cellular components of blood (Rooney

et al. 1972). One component thought to be the cause is direct shearing stress, which microbubbles cause when they expand.

Direct shearing stresses and oscillating shearing stresses, which form near rigid boundaries associated with the expansion and contraction of microbubbles have been shown to be essential in biological effects of hemoglobin release of blood cell suspensions (Nyborg et al. 1982). Vibrating bubbles under traditional diagnostic ultrasound have also been shown to cause human blood to release platelets and other cellular molecules such as ATP (Williams et al. 1973). It has also been shown that the biological effects of microstreaming can destroy cells due to the rapid stretching that shearing fields cause, thus resulting in cell membrane rupture, although only cells within the immediate vicinity of the shearing activity are affected (NCRP 2002).

Both the oscillating wire and the oscillating gas bubble experiments support the hypothesis that acoustic streaming mechanisms are important stresses that cause the destruction of red blood cells. Furthermore, the same effect was generated with two different microstreaming causing sources—an oscillating rigid wire and an oscillating gas bubble. With this original concept, recent studies have shown that the inclusion of microbubbles that can undergo oscillations and therefore cause microstreaming increase the thrombolytic effect when exposed to ultrasound (Tachibana et al. 1995; Prokop et al. 2007). Although the mechanisms of action are unknown or, at best, poorly understood, the effect is real and has been well documented.

Microstreaming phenomena occur when a microbubble, surrounded by a liquid media, undergoes direct oscillatory action when exposed to ultrasound. Oscillatory action causes rapid, toroidal eddy currents to form as a result of the displacement of

liquid around the bubble. These eddy currents decrease in size as the ultrasonic frequency is increased (NCRP 2002); that is, less microstreaming occurs at higher frequencies. Microstreaming, therefore, is a consequence of low-frequency, low-pressure response to oscillations of microbubbles.

Previous studies into contrast agent-enhanced thrombolysis fail to examine important factors such as frequency and pressure dependence on microstreaming, focusing only on a single frequency or a single pressure. Few studies have investigated the range of pressures and frequencies to discover the exact mechanism by which microbubbles enhance the effect of thrombolysis. It is the hypothesis of this investigation, and thus the purpose of the rest of this thesis, that the oscillatory response of microbubbles and the resulting microstreaming effect produced is the primary mechanism by which contrast agents enhance thrombolysis. A frequency spectrum of 395 kHz, 545 kHz, 790 kHz, and 1.02 MHz with a pressure range of 8 kPa to 0.5 MPa will be used in order to examine the effects that microstreaming may have on thrombolysis.

CHAPTER 6: MATERIALS

This section describes the materials used to perform the experiments. The materials, which will be described in more detail, are the experimental tank, power source, membrane hydrophone, heating control unit, human blood, and Definity contrast agent. Block diagrams of the calibration and characterization procedures as well as the experimental set-up will be described in Chapter 7.

6.1 Experimental Tank

A custom Lucite tank was built by the Electrical Engineering Machine Shop of the University of Illinois at Urbana-Champaign, with measurements of $68 \times 28 \times 30$ cm and a thickness of 1.5 cm. It was fixed with two rails on the longitudinal axis to allow for objects within the tank to be translated laterally and longitudinally. It was sealed using a water-resistant, clear-coated adhesive and tested to be watertight.

6.2 Power Source

An Agilent 33250A, 80 MHz digital-function generator was used to create the sinusoidal input to the transducer. The output of the function generator was fed into a 60 dB, 500 RF Power Amplifier (ENI Inc., Rochester, NY), which had a band-pass filter of 0.3 to 35 MHz. The output of the power amplifier was then connected to the source transducer.

6.3 Hydrophone

The source transducer was calibrated using a polyvinylidene fluoride (PVDF) Marconi membrane hydrophone manufactured by Marconi and Caswell Technology.

The Marconi hydrophone consists of a coplanar, monolayer of thin PVDF film, 100 mm in diameter, with a piezoelectrically active central area roughly 0.5 mm in diameter. The output voltage is proportional to the pressure at that point in the ultrasonic field. The hydrophone interfaces with monitoring systems via a matched amplifier and 75 ohm BNC cable connections.

The calibration of the hydrophone was performed by the National Physical Laboratory of Teddington, Middlesex, United Kingdom, using a multiple-frequency method by direction comparison with a secondary standard hydrophone of the membrane type (NPL calibration sheet). The calibration was performed in two distinct stages, the first being from 1 to 20 MHz, incrementing by 1 MHz each step. The second was a fine-frequency calibration from 0.3 to 0.9 MHz, with an 0.1 MHz incrementation. The calibration was carried out in fresh, de-ionized water at 20.9°C to 21.4°C, with a standard deviation of $\pm 0.5^\circ\text{C}$, using a tone-burst excitation swept through the calibrated frequencies.

6.4 Heating Controller

Two 100 W, floor-mounted heaters were used to heat the degassed water to 37°C. The heaters were controlled by a 117 V, 10 A, 60 Hz proportional temperature controller (Yellow Springs Instrument Co., Yellow Springs, OH). To ensure even distribution of heat throughout the tank, a 120 VAC, 698 W, 60 Hz Corning stirrer/hotplate, model PC 420, was placed beneath the Lucite tank and stirred with a magnetic stir-bar set to the lowest setting, which was measured to be approximately 120 rpm.

6.5 Transducers

The transducers were single-element transducers consisting of a custom-built fixture (Figure 6.1a), manufactured by the Electrical Engineering Machine Shop at the University of Illinois at Urbana-Champaign. Unfocused crystals with center frequencies of 395 kHz, 545 kHz, 790 kHz, and 1.02 MHz from Valpey Fischer Inc., with an active surface of diameter 20 mm were used. The housing for the single-element transducer consisted of a cylindrical stainless steel alloy with the crystal sealed to the housing with anodized aluminum. It was then grounded electrically to the housing to ensure that no electrical grounding occurred within the element. Within the housing, a gold-plated bromine-copper (BrCu), shown in Figure 6.1.1b, fixed to a Bayonet Neill Concelman (BNC) connector was mounted to excite the crystal (Figure 6.1b). Electrical connectivity was ensured, and a washer was placed between the housing and the outside to waterproof the interior of the transducer. It was then sealed and tightened with four hex screws. The calibration and characterizations of the transducers will be described in Chapter 7.

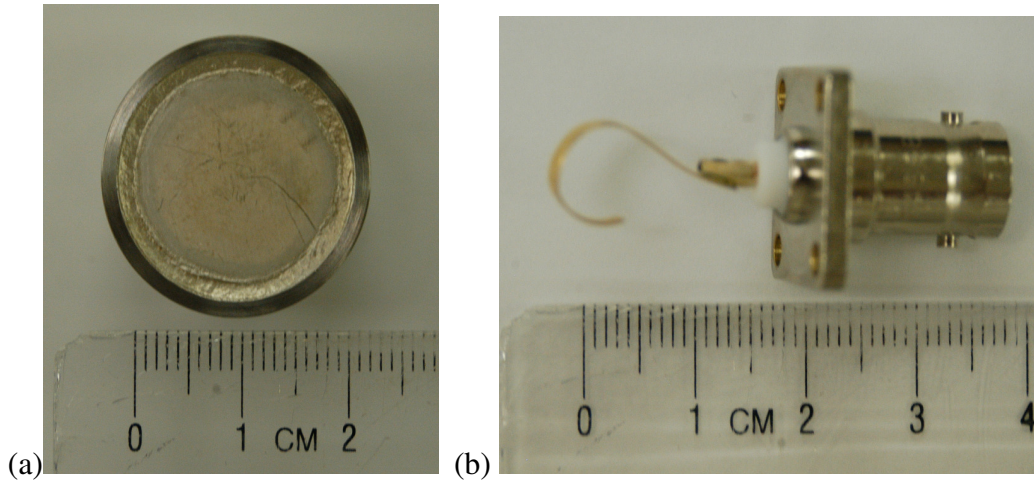


Figure 6.1. (a) Housed transducer crystal, (b) BrCu within transducer housing.

6.6 Blood

Samples of whole blood clots were acquired from Community Blood Services of Urbana, Illinois, in unmarked tubes for privacy purposes. Each sample was tested for the following bloodborne pathogens prior to being released, as required by the U.S.

Food and Drug Administration:

- hepatitis B surface antigen
- hepatitis B core antibody (total)
- HCV 2.0 antibody screen
- HCV NAT
- HIV-1/HIV-2 antibody screen
- HIV NAT
- HTLV-I/HTVL-II antibody screen
- WNV NAT
- RPR screen ASI syphilis
- CMV antibody screen

- ABO and Rh groups for typing.

Possible adverse health conditions of the blood donors were not addressed because each donor had been determined medically healthy to donate blood by the appropriate medical staff. Therefore, each sample is considered a random sample from a uniform population. The acquisition and use of human blood was approved by the Institutional Review Board and the Division of Research Safety of the University of Illinois.

6.7 Ultrasound Contrast Agent

Ultrasound contrast agent (UCA) was used to study the effects of microstreaming on thrombolysis at a concentration of 0.1 mL per 4 mL of degassed water. This concentration ensured complete saturation of contrast agent with the blood while preventing the bubbles from shielding any ultrasound pressure. The contrast agent used was Definity. Prior to activation, the vial contains a clear, colorless, sterile, non-pyrogenic, hypertonic liquid, which upon activation yields perflutren lipid microspheres. The resulting solution is a homogenous, opaque, milky-white injectable suspension. According to instructions for use of Definity in a clinical setting, this solution is injected intravenously, allowed to circulate, and then imaging is done (Definity 2008). However, for the purposes of this investigation, the contrast agent was injected into degassed water to form a homogenous solution.

Definity consists of perflutren lipid microspheres composed of octafluoropropane that are encapsulated in an outer lipid shell consisting of (R)-hexadeconic acid, 1-[(phosphonoxy)methyl]-1,2-ethanediyl ester, monosodium salt (DPPA); (R)-4-hydroxy-N,N,N-trimethyl-10-oxo-7-[(1-oxohexadecyl)oxy]-3,4, 9-trioxa-4- phosphapentacosan-1-aminium, 4-oxide, inner salt (abbreviated DPPC); and

(R)- α -[6-hydroxy-6-oxido-9-[(1-oxohexadecyl)oxy]-5,7,11-trioxa-2-aza-6-phosphahexacos-1-yl]- ω -methoxypoly (ox-1,2-ethanediyl), monosodium salt (abbreviated MPEG5000 DPPE).

After activation, each milliliter of the milky-white suspension is reported to contain about 150 μ L per mL of octafluoropropane and a maximum of 1.2×10^{10} perflutren lipid microspheres with a mean radius of 1.1 to 3.3 μ m.

CHAPTER 7: METHODS

The following section describes the methods and procedures for transducer calibration, characterization, and experimental set-up. All calibrations, characterizations and experiments were performed at 37°C in degassed, fresh water.

7.1 Transducer Calibration and Characterization Procedure

Each transducer was characterized prior to the beginning of the study to determine transducer beam characteristics. Each transducer was calibrated before and after a set of experiments using the same power amplifier, function generator, and cables to minimize variability and ensure consistency. The calibration and characterization procedures follow routine and established protocols so that they may be repeated and remain consistent regardless of the researcher performing them.

7.1.1 Center Frequency Measurement

To obtain the center frequencies of each transducer, each was mounted perpendicularly to the Marconi membrane hydrophone. A Panametrics model 5800 pulsing source was used to send a broadband pulse to each transducer. The signal was displayed on a LeCroy model 5600 digital oscilloscope with a sampling rate of 500 Ms/s. The fast Fourier transform, FFT, was taken from the hydrophone signal and the center frequencies of each transducer were measured.

7.1.2 Calibration Procedure

To calibrate each transducer, the Marconi membrane hydrophone was at the last axial maximum (LAM) of the beam of the transducer calculated by Kinsler et al. (2000):

$$LAM = \frac{a^2}{\lambda} - \frac{\lambda}{4}. \quad (7.1)$$

This distance is specific to each transducer. Using a multitranslational positioning system by Daedal Systems Inc., the Marconi membrane hydrophone was placed in the center of the beam and its symmetry checked. This was done by moving the hydrophone vertically in equal and opposite distances from a starting point and measuring the amplitude decrease. If the amplitude decreased the same amount over each distance, the transducer was considered to be vertically centered with respect to the hydrophone. If the amplitude decrease was not the same, proper adjustments were made to the fixed starting point and the process was repeated. The same process was then performed by moving the hydrophone laterally and measuring the amplitude decrease. Once the amplitude decreased the same amount for equal distances, it was considered to be positioned centered laterally. Routine calibration using this method resulted in approximately a 5% error in all calibrations.

Following the centering procedure, the function generator was swept through the desired voltages, and each waveform was captured digitally. A custom MATLAB program analyzed each waveform and calculated the peak compressional and peak rarefractional (P_c and P_r) pressures. Owing to their more consistent response at higher pressures, only peak rarefractional pressures are reported.

Because of the spatial variability of the near field of unfocused transducers, the last axial maximum (LAM) was chosen for calibration. This location marks the transition from the variable near field to the far field, which is more uniform and predictable for consistent calibrations (Kinsler et al. 2000). Figure 7.1 shows a Field II simulation of the axial pressure magnitude from a 1.02 MHz source. As can be seen, the near field is considerably variable where the far field, marked by the last axial maximum at 66.3 mm, is a smoother and more uniform curve, eventually approaching $\frac{1}{r}$ decay. Pressure calibration curves for each transducer can be found in Appendix I.

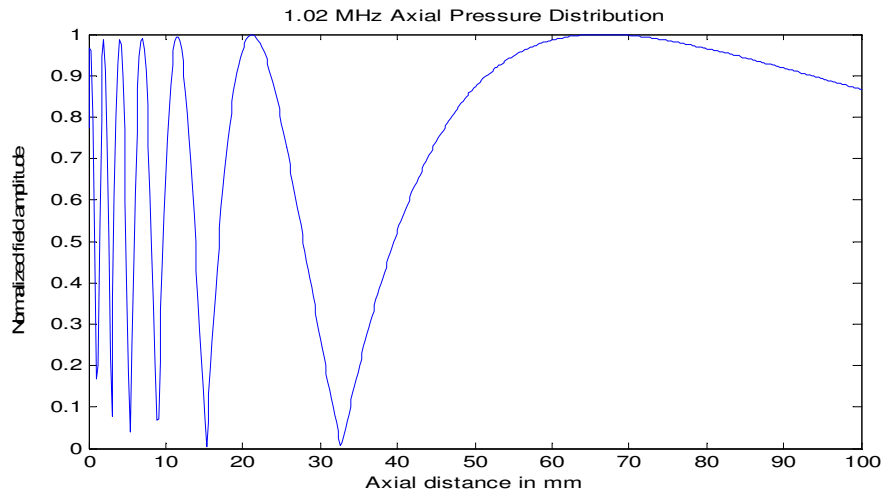


Figure 7.1. Field II simulation showing axial pressure distribution.

7.1.3 Characterization Procedure

To obtain beam characteristics of each transducer, the Marconi membrane hydrophone was placed at the last axial maximum of the beam of the transducer as calculated by Equation 7.1, and the symmetry was checked to ensure that the active reaction of the hydrophone was in the geometrical center of the transducer beam. The hydrophone was laterally moved out of the beam until the amplitude decreased to noise

level. The hydrophone was then laterally translated 22 mm across the center of the beam using 0.05 mm steps, for a total of 440 lateral scan segments. The amplitude was observed to gradually peak in the center of the beam and then decrease until it reached noise level. Each of the 440 lateral waveform segments were recorded, compiled, and analyzed using a custom MATLAB program. A block diagram of the calibration and characterization set-up is depicted in Figure 7.2.

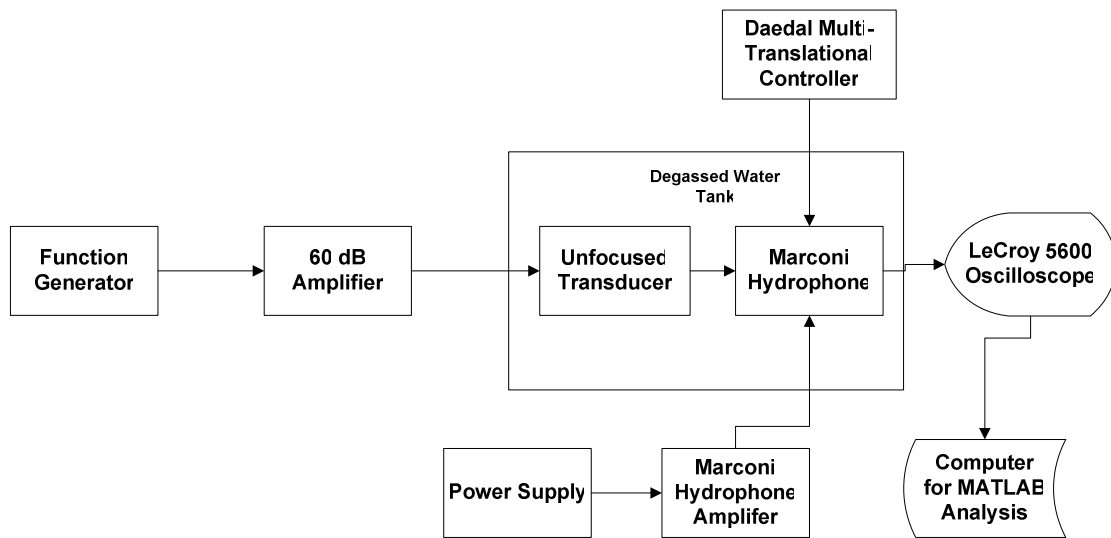


Figure 7.2. Block diagram of calibration and characterization set-up.

Beam characteristics of each transducer were calculated, including wavelength, last axial maximum distance, -6 dB beamwidth, and -10 dB beamwidth, as listed in Table 7.1. With a blood clot sample diameter of 5.8 ± 0.5 mm, the -6 dB beamwidth of each transducer was greater than the size of the sample clot. Beam figures can be found in Appendix II.

Frequency	395 kHz	545 kHz	790 kHz	1.02 MHz
Wavelength	3.86 mm	2.78 mm	1.93 mm	1.49 mm
LAM	25.91 mm	35.76 mm	51.83 mm	66.3 mm
-6 dB Beamwidth	6.6 mm	12.5 mm	10.7 mm	10.8 mm
-10 dB Beamwidth	Not measurable	22.3 mm	15 .2 mm	14.5 mm

Table 7.1. Calculated beam characteristics of custom made, unfocused transducers.

7.2 Blood Clot Preparation

All blood samples acquired from Community Blood Services of Illinois were randomly chosen by a laboratory technician over the course of the study’s six-month period. Experiments were performed and validated by three independent researchers. Blood samples were released after being tested for all major bloodborne pathogens as required by the FDA. Blood used was reported to be approximately 7 to 10 days old. Use of human blood was approved by the Instructional Review Board and the Division of Research Safety of the University of Illinois.

Whole human blood clots were prepared by evacuating approximately 3 mL of human venous blood into 10 mm diameter plastic tubes by Community Blood Services of Illinois. The evacuated tubes contained no anticoagulants, and blood clotted at room

temperature within minutes. Blood clot tubes were kept at room temperature for 3 to 5 hours while testing was completed. Prior to their initial testing for bloodborne pathogens, each tube was spun at 2,000 rpm for 5 minutes to extract plasma. After the plasma was extracted, the clot tubes were stored at 4°C. After the plasma was tested and determined to be safe, the blood was released for experimentation. The received tubes contained a fully retracted clot.

The fully retracted blood clot weighed approximately 1,200 mg. It was extracted from the plastic tube from which it was originally stored and was cut using a razor blade into four equally sized pieces weighing approximately 300 mg each. Each 300 mg sample was then cut into two samples, roughly 150 mg each. These 150 mg pairs served as an exposure sample and a matched control sample. Exposed samples had two different classifications: samples exposed to ultrasound only and samples exposed to ultrasound and contrast agent. Each exposed sample had a matched control that did not undergo any ultrasound exposure. Figure 7.3 is a flow diagram that depicts the cutting procedure.

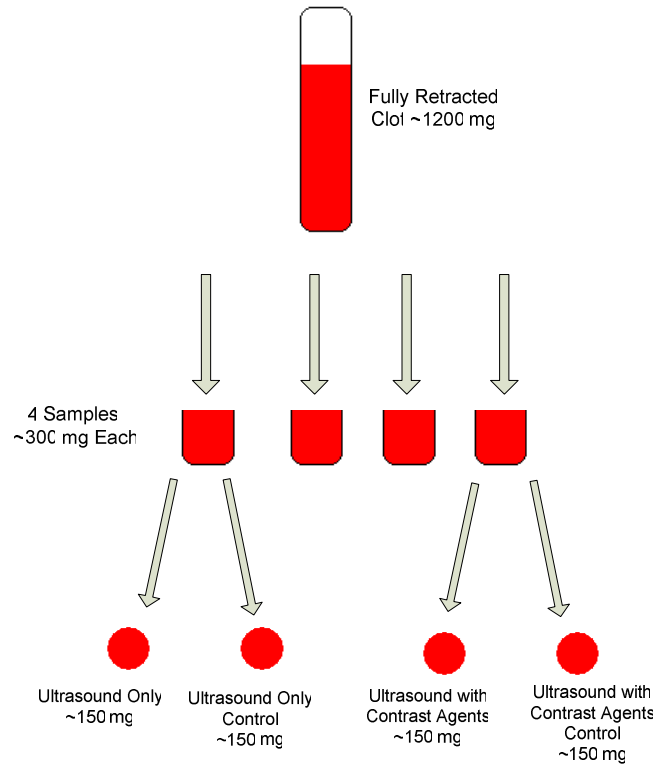


Figure 7.3. Flow diagram of clot cutting process.

The surfaces as well as the edges of all samples were trimmed to eliminate any overly fibrous portion that may have developed along the surface of the tube in which it was housed. After extraction, the samples were weighed on a digital scale that had an accuracy of 0.01 mg, and their weights were recorded. The clots were then placed in a self-sealing, acoustically permeable, plastic jewelry bag (Crafts, Etc.), measuring 5.08 × 7.62 cm with 4 mL of degassed water at 37°C.

7.3 Definity® Preparation

The commercially available contrast agent Definity was used in this study as the ultrasound contrast agent. Definity comes in a 2 mL, clear glass vial. Prior to use, the vial was activated using the published activation protocol. The vial was allowed to

warm to room temperature and activated by shaking it for 45 seconds using a Vialmix®. 0.1 mL of Definity contrast agent was diluted by 4 mL of degassed water and placed the acoustically permeable bag prior to addition of the sample clot. 0.1 mL of Definity corresponds to approximately 1.2×10^9 perflutren lipid microspheres (Definity 2008).

7.4 Experimental Procedure

There were four different experimental cases for each exposure. The first and second cases consisted of a sample exposed to continuous wave (CW) ultrasound for 15 minutes in 37°C, degassed water and its matched control sample, which did not undergo ultrasound exposure but remained in 37°C, degassed water for 15 minutes. The third and fourth cases consisted of a sample exposed to CW ultrasound and Definity contrast agent for 15 minutes in 37°C, degassed water and its control sample, which did not undergo ultrasound exposure but remained in 37°C, degassed water for 15 minutes. The bag containing the sample for exposure was visually aligned to the center of the transducer beam and placed axially at the last axial maximum. Additionally, the control sample of similar size and weight was placed in a similar, acoustically permeable bag and placed in a 37°C, degassed water bath without being exposed to ultrasound.

Time was kept using a digital timer and was started when the acoustically permeable bag was placed in the transducer beam and the source was turned on. Timing stopped when the source was turned off. A small magnetic stir-bar set at approximately 180 rpm gently agitated the water and kept the water heated evenly. A digital thermometer was placed near the site of exposure to monitor and ensure the temperature was 37°C.

After the exposure time, both the exposed sample and the control sample were placed on an 11 × 21 cm 1-ply, Delicate Task Wipes (Kimberly-Clark) and dried through capillary action and light blotting (Holland et al., 2008). The samples were weighed again and their weights recorded. The same procedure was used for samples containing contrast agent. 0.1 mL of Definity contrast agent was injected into 4 mL of degassed water prior to the placement of the sample in the permeable bag. The same concentration of Definity was injected into the control bag. The experimental set-up is depicted in Figure 7.4.

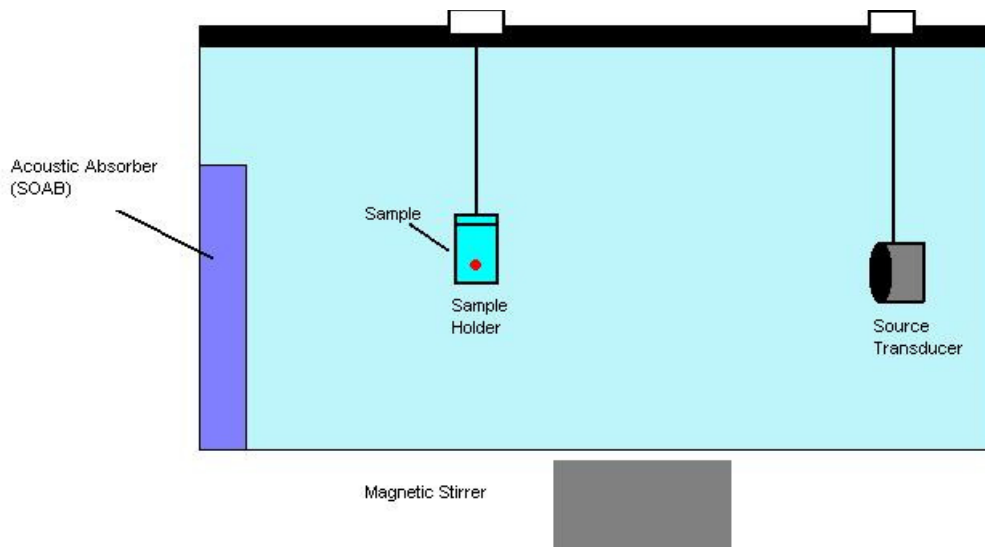


Figure 7.4. Experimental set-up with the sample clot placed at the last axial maximum.

7.5 Statistical Analysis and Mass Loss Relative to Matched Control

Samples undergoing ultrasound exposure and their matched controls were weighed before and after the 15 minute exposure duration and their mass losses calculated by

$$\Delta M_{US} = M_{ie(US)} - M_{fe(US)} \quad (7.2)$$

$$\Delta M_{US+UCA} = M_{ie(US+UCA)} - M_{fe(US+UCA)} \quad (7.3)$$

$$\Delta M_{c(US)} = M_{ic(US)} - M_{fc(US)} \quad (7.4)$$

$$\Delta M_{c(UCA)} = M_{ic(UCA)} - M_{fc(UCA)}. \quad (7.5)$$

Equation 7.2 represents the mass loss of samples exposed to ultrasound only where ΔM_{US} is the change in mass of samples exposed to ultrasound only, $M_{ie(US)}$ is the initial mass of the sample exposed to ultrasound only, and $M_{fe(US)}$ is the final mass of the sample exposed to ultrasound only. Equation 7.4 represents the mass loss of matched control samples not exposed to ultrasound. $\Delta M_{c(US)}$ is the change in mass of the control sample, $M_{ic(US)}$ is the initial mass of the control sample, and $M_{fc(US)}$ is the final mass of the control sample. ΔM_{US+UCA} (Equation 7.3) represents the mass loss of samples exposed to ultrasound and Definity contrast agent. $M_{ie(US+UCA)}$ is the initial mass of samples exposed to ultrasound and Definity contrast agent, and $M_{fe(US+UCA)}$ is the final mass of samples exposed to ultrasound and Definity contrast agent. Equation 7.5 represents the change in mass loss of the control samples with Definity contrast agent present. $\Delta M_{c(UCA)}$ represents the change in mass loss of the control sample, $M_{ic(UCA)}$ is the initial mass of the control sample with contrast agent, and $M_{fc(UCA)}$ is the final mass of the control sample with contrast agent.

Relative mass loss of samples compared to their matched control for samples exposed to ultrasound only, $M_{r(US)}$, and samples exposed to ultrasound and contrast agent, $M_{r(US+UCA)}$, were calculated by subtracting the change in mass loss of the respective control samples, $\Delta M_{c(US)}$ and $\Delta M_{c(UCA)}$, from the change in mass loss of the corresponding exposed samples, $\Delta M_{(US)}$ and $\Delta M_{(US+UCA)}$, and normalized to the appropriate control sample.

$$M_{r(US)} = \frac{\Delta M_{(US)} - \Delta M_{c(US)}}{\Delta M_{c(US)}} \quad (7.6)$$

$$M_{r(US+UCA)} = \frac{\Delta M_{(US+UCA)} - \Delta M_{c(UCA)}}{\Delta M_{c(UCA)}}. \quad (7.7)$$

A total of six relative mass loss of samples compared to their matched control trials for samples exposed to ultrasound only, $M_{r(US)}$, and samples exposed to ultrasound and contrast agent, $M_{r(US+UCA)}$, were performed for each exposure pressure of 8, 19, 32, 40, 50, 120, 300, and 550 kPa at four individual frequencies of 395 kHz, 545 kHz, 790 kHz, and 1.02 MHz. The six values for $M_{r(US)}$ and $M_{r(US+UCA)}$ were then averaged and their standard deviations calculated to obtain average relative mass losses represented by

$$\overline{M}_{r(US)} = \frac{1}{n} \sum_6 M_{r(US)}(n) \quad (7.8)$$

$$\overline{M}_{r(US+UCA)} = \frac{1}{n} \sum_6 M_{r(US+UCA)}(n). \quad (7.9)$$

with n being the trial number, and $M_{r(US)}$ and $M_{r(US+UCA)}$ being the relative mass losses found in Equations 7.6 and 7.7.

Each control sample and exposed sample were matched to each other (that is, they were taken from the same piece of clotted blood); therefore, it is assumed that both samples have the same cellular properties of stiffness, rigidity, and platelet characteristics. Matched control samples for Definity trials contained the same amount of Definity contrast agent as did the matched ultrasonically exposed sample: 0.1 mL per 4 mL of degassed water.

Statistical analysis was done on the individual relative mass losses found in Equations 7.6 and 7.7. A one-tailed student's t-test analysis was used with an alpha level of 0.05, corresponding to a t-value of 2.776. The null hypothesis tested, H_0 , was the average relative mass loss of samples exposed to ultrasound only and was equal to the average relative mass loss of samples exposed to ultrasound and Definity contrast agent; there was no significant mass loss with the addition of Definity contrast agent. The alternative hypothesis, H_1 , was the average relative mass loss of samples exposed to ultrasound and was not equal to the average relative mass loss of samples exposed to ultrasound and Definity contrast agent; the addition of Definity contrast agent has a significant effect on relative mass loss. A t-test value that is greater than the test statistic value, 2.776, or a probability less than the alpha level of 0.05 is considered statistically significant and the null hypothesis, H_0 , is rejected and the alternative hypothesis, H_1 is accepted with a 0.05 probability of committing a Type 1 error.

7.6 Theoretical Bubble Displacement and Viscous Shear Stress Calculations

To estimate the displacement amplitudes of Definity under the exposed experimental pressures of 8, 19, 32, 40, 50, 120, 300, and 550 kPa, a theoretical model was developed by solving the Marmottant equation (Marmottant et al. 2005) for large-amplitude oscillations of coated microbubbles:

$$\rho_l \left(R\ddot{R} + \frac{3}{2}\dot{R}^2 \right) = \left[P_0 + \frac{2\sigma(R_0)}{R_0} \right] \left(\frac{R}{R_0} \right)^{-3\kappa} \left(1 - \frac{3\kappa}{c} \dot{R} \right) - P_0 - \frac{2\sigma(R)}{R} - \frac{4\mu\dot{R}}{R} - \frac{4\kappa_s\dot{R}}{R^2} - P_{ac}(t). \quad (7.10)$$

Equation 7.10 was chosen because it describes the theoretical bubble dynamics of a lipid sphere, which most resemble the contrast agent Definity. In Equation 7.10, R_0 is the equilibrium radius of the bubble, ρ_l is the density of the medium, P_0 is the ambient pressure, $\sigma(R)$ is the effective surface tension, κ is the polytropic gas exponent, κ_s is the shell surface viscosity, c is the speed of sound in the medium, and $P_{ac}(t)$ is the acoustic pressure. The surface tension, $\sigma(R)$, is expressed in terms of the bubble radius with three specific conditions:

$$\sigma(R) = \begin{cases} 0 & \text{if } R \leq R_{buckling} \\ \chi \left(\frac{R^2}{R_{buckling}^2} - 1 \right) & \text{if } R_{buckling} \leq R \leq R_{break-up} \\ \sigma_{water} & \text{if ruptured and } R \geq R_{ruptured} \end{cases}, \quad (7.11)$$

where χ is the elastic modulus of the elastic regime of the bubble; $R_{buckling}$ is the radius below which the surface of the microbubble buckles; $R_{break-up}$ is the radius above which the surface shell breaks up, described as $R_{buckling}(1+\sigma_{break-up}/\chi)^{1/2}$; σ_{water} is the surface tension of water; and $R_{ruptured}$ is the radius after rupture, described as $R_{buckling}(1+\sigma_{water}/\chi)^{1/2}$. It should be noted that the simulated bubble displacement

amplitudes never show bubble collapse. It was observed that at pressures of 300 and 550 kPa, there was no visible Definity remaining in the sample bags.

The ordinary differential equation solver in MATLAB was used to solve the Marmottant equation, Equation 7.10, by solving for the changing radius of a bubble over time. Experimental parameters and estimated lipid shell parameters that best mimicked Definity were used in the solution and are listed in Table 7.2 (Marmottant et al. 2005). To simulate continuous-wave pulsing, a pulse duration of 15 cycles was used. A 15-cycle pulse was chosen for processing time purposes and because no significant differences in bubble displacement amplitudes was seen at pulse durations greater than 15 cycles.

Parameter	Value	Description
ρ_l	992 kg/m ³	For fresh water at 37°C
P_0	101 kPa	Atmospheric pressure
R_0	1.65 μ m	Mean radius for Definity 0.55–1.65 μ m
κ	1.07	For perflouropropane
κ_s	0.5x10 ⁻⁹ N for Definity	Definity (Goertz et al. 2007)
c	1524 m/s	For fresh water at 37°C
$P_{ac}(t)$	$P_r \sin(2\pi ft)$	Sinusoidal pulse
f	395 kHz, 545 kHz, 790 kHz, 1.02 MHz	
$R_{buckling}$	R_0	(Marmottant et al. 2005)
χ	0.85 N/m for Definity	Definity (Goertz et al. 2007)
$R_{breakup}$	$R_{buckling}(1+\sigma_{break-up}/\chi)^{1/2}$	(Marmottant et al. 2005)
$\sigma_{break-up}$	1 N/m	(Marmottant et al. 2005)
$R_{ruptured}$	$R_{buckling}(1+\sigma_{water}/\chi)^{1/2}$	(Marmottant et al. 2005)
σ_{water}	0.073 N/m	

Table 7.2. Parameters used in Definity bubble displacement simulation.

The goal of this research is to determine whether microstreaming and its induced oscillatory viscous shear stresses caused by oscillatory bubble displacement are

responsible for enhanced thrombolysis over controls. If the bubble displacement amplitudes for the various exposure conditions are known, $R - R_0$, the associated oscillatory shear viscous stresses, S_c , can be calculated by finding the acoustic streaming velocity gradient, G (Nyborg et al. 1964):

$$G = \frac{2\pi f (R - R_0)^2}{R_0 \left(\frac{\eta}{\pi \rho_l f} \right)^{\frac{1}{2}}}, \quad (7.12)$$

where f is the driving frequency and η is the coefficient of shear viscosity of medium.

Because the radius of the bubble, R , changes with time, R_{\max} will be the radius used for R in solving for the acoustic streaming velocity gradient (Equation 7.12). The oscillatory viscous shear stress, S_c , can be calculated by multiplying the viscosity of the medium by the acoustic streaming velocity gradient, G (Nyborg et al. 1964):

$$S_c = \eta G. \quad (7.13)$$

The simulated results for S_c can be found in Table 8.4.2. The solution to the Marmottant equation simulates oscillatory bubble displacement amplitudes for a single, fixed-diameter bubble. However, commercial Definity contrast agent has wide-ranging bubble diameters, and the amount of Definity bubbles used was greater than a single bubble. Because of the limited research in this area, the rough estimates for the parameters were chosen to give an accurate representation into the bubble dynamics.

CHAPTER 8: RESULTS

The purpose of this thesis, as previously stated, is to examine the pressure and frequency dependence of microstreaming, which current literature is lacking. Showing these dependencies can aid further research into the areas of contrast agent–enhanced thrombolysis by narrowing in on the most effective and efficient methods. Exposure pressures examined were 8, 19, 32, 40, 50, 120, 300, and 550 kPa at frequencies of 395 kHz, 545 kHz, 790 kHz, and 1.02 MHz. The average relative mass losses, $\overline{M}_{r(US)}$ and $\overline{M}_{r(US+UCA)}$, found in Equations 7.8 and 7.9, are presented along with the standard deviations. Samples exposed to ultrasound only are depicted on the left of the two columns (blue), and samples exposed to ultrasound and contrast agent are on the right of the two columns (orange), as shown later in Figure 8.1.

8.1 Tables of Results

Tables 8.1 through 8.4 show the average relative mass losses, $\overline{M}_{r(US)}$ and $\overline{M}_{r(US+UCA)}$, found in Equations 7.8 and 7.9 for each acoustic pressure (column 1) for samples exposed to ultrasound only (column 2) and samples exposed to ultrasound and 0.1 mL of contrast agent (column 3) for four exposure frequencies, 395 kHz, 545 kHz, 790 kHz, and 1.02 MHz. Mass losses are presented as percentages with the standard deviation in parenthesis. A one tailed t-test was performed and statistical significance was determined between samples exposed to ultrasound and samples exposed to ultrasound and Definity with a significance level of $\alpha = 0.05$ (column 4). Alpha values less than 0.05 were considered statistically significant, while values greater than 0.05 were not considered significant (column 5).

395 kHz

Pressure	Ultrasound Only Mass Loss% (Standard Deviation)	Ultrasound and UCAs Mass Loss% (Standard Deviation)	P value of T-Test Statistic	Statistically Significant (Y/N)
8 kPa	-0.69 (1.94)	-0.25 (2.22)	0.359	N
19 kPa	50.96 (23.07)	85.46 (11.00)	0.001	Y
32 kPa	53.86 (17.46)	65.10 (10.87)	0.108	N
40 kPa	17.58 (3.56)	27.36 (9.16)	0.024	Y
50 kPa	58.54 (23.07)	61.39 (3.20)	0.394	N
120 kPa	41.38 (22.14)	63.40 (8.66)	0.013	Y
300 kPa	0.71 (1.21)	0.33 (0.97)	0.284	N
550 kPa	0.79 (1.69)	0.37 (1.11)	0.341	N

Table 8.1. Relative mass losses at 395 kHz.

545 kHz

Pressure	Ultrasound Only Mass Loss% (Standard Deviation)	Ultrasound and UCAs Mass Loss% (Standard Deviation)	P value of T-Test Statistic	Statistically Significant (Y/N)
8 kPa	2.29 (3.28)	-0.25 (2.22)	0.245	N
19 kPa	29.59 (5.29)	85.46 (11.00)	~0.00	Y
32 kPa	23.90 (10.31)	65.10 (10.87)	~0.00	Y
40 kPa	16.23 (7.19)	31.84 (13.01)	0.017	Y
50 kPa	34.65 (17.91)	61.39 (3.20)	0.011	Y
120 kPa	30.85 (14.95)	63.40 (8.66)	0.003	Y
300 kPa	0.10 (1.84)	0.33 (0.97)	0.168	N
550 kPa	0.58 (4.93)	0.37 (1.11)	0.454	N

Table 8.2. Relative mass losses at 545 kHz.

790 kHz

Pressure	Ultrasound Only	Ultrasound and UCAs	P value of T-Test Statistic	Statistically Significant (Y/N)
	Mass Loss% (Standard Deviation)	Mass Loss% (Standard Deviation)		
8 kPa	-0.80 (1.24)	0.69 (1.70)	0.089	N
19 kPa	24.82 (5.66)	43.66 (21.40)	0.042	Y
32 kPa	33.69 (12.34)	50.57 (18.29)	0.047	Y
40 kPa	17.16 (3.34)	20.64 (5.90)	0.039	Y
50 kPa	25.40 (16.89)	50.67 (20.05)	0.020	Y
120 kPa	27.28 (22.25)	51.72 (18.69)	0.034	Y
300 kPa	9.14 (6.60)	2.88 (3.58)	0.099	N
550 kPa	1.06 (2.86)	1.94 (1.10)	0.246	N

Table 8.3. Relative mass losses at 790 kHz.

1.02 MHz

Pressure	Ultrasound Only	Ultrasound and UCAs	P value of T-Test Statistic	Statistically Significant (Y/N)
	Mass Loss% (Standard Deviation)	Mass Loss% (Standard Deviation)		
8 kPa	0.15 (1.96)	-0.64 (0.68)	0.193	N
19 kPa	32.19 (7.69)	67.53 (3.00)	1.06 E-05	Y
32 kPa	33.60 (3.25)	71.47 (5.38)	1.70 E-07	Y
40 kPa	13.16 (2.78)	20.58 (2.84)	4.42 E-04	Y
50 kPa	32.75 (5.46)	68.31 (2.40)	9.95 E-07	Y
120 kPa	31.97 (5.83)	68.88 (4.33)	2.22 E-07	Y
300 kPa	0.55 (1.46)	0.34 (2.68)	0.436	N
550 kPa	-0.50 (1.27)	0.086 (2.70)	0.321	N

Table 8.4. Relative mass losses at 1.02 MHz.

8.2 Average Relative Mass Loss for Various Pressures

Figures 8.1 through 8.4 show the relative mass losses, $\overline{M}_{r(US)}$, $\overline{M}_{r(US+UCA)}$, calculated in Equations 7.8 and 7.9, respectively, for frequencies of 395 kHz, 545 kHz, 790 kHz, and 1.02 MHz. The sample size was six; the peak rarefractional pressure values are in kilopascals, kPa; and the average relative mass losses are percentages.

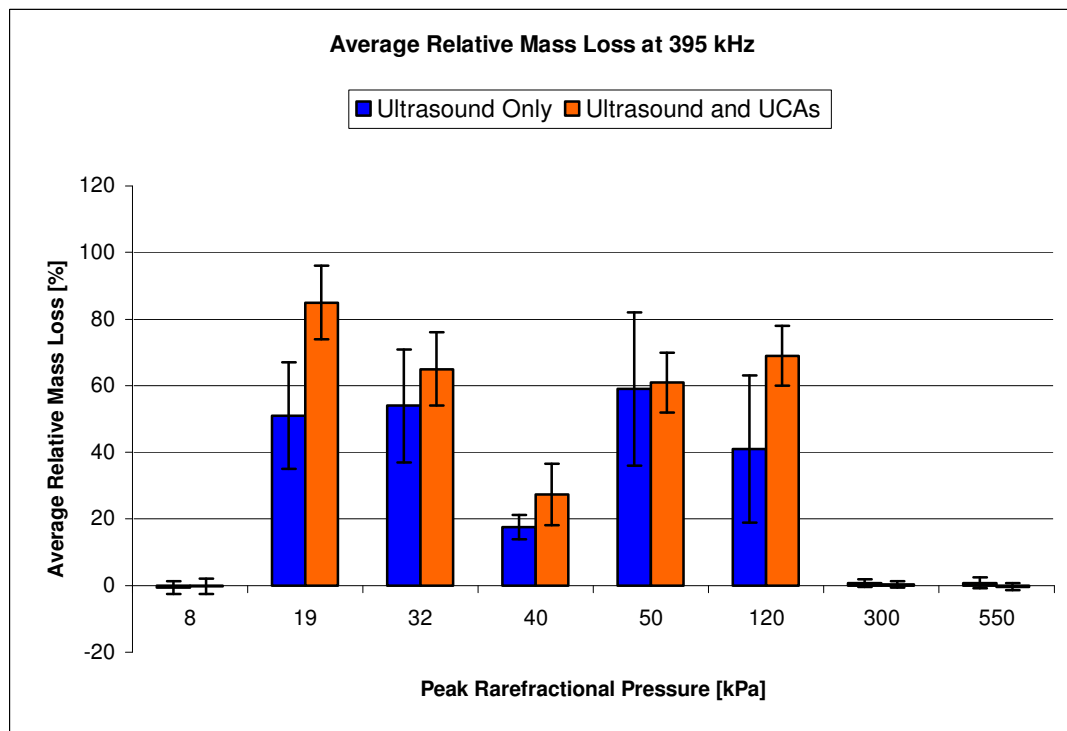


Figure 8.1. Average relative mass loss at a frequency of 395 kHz.

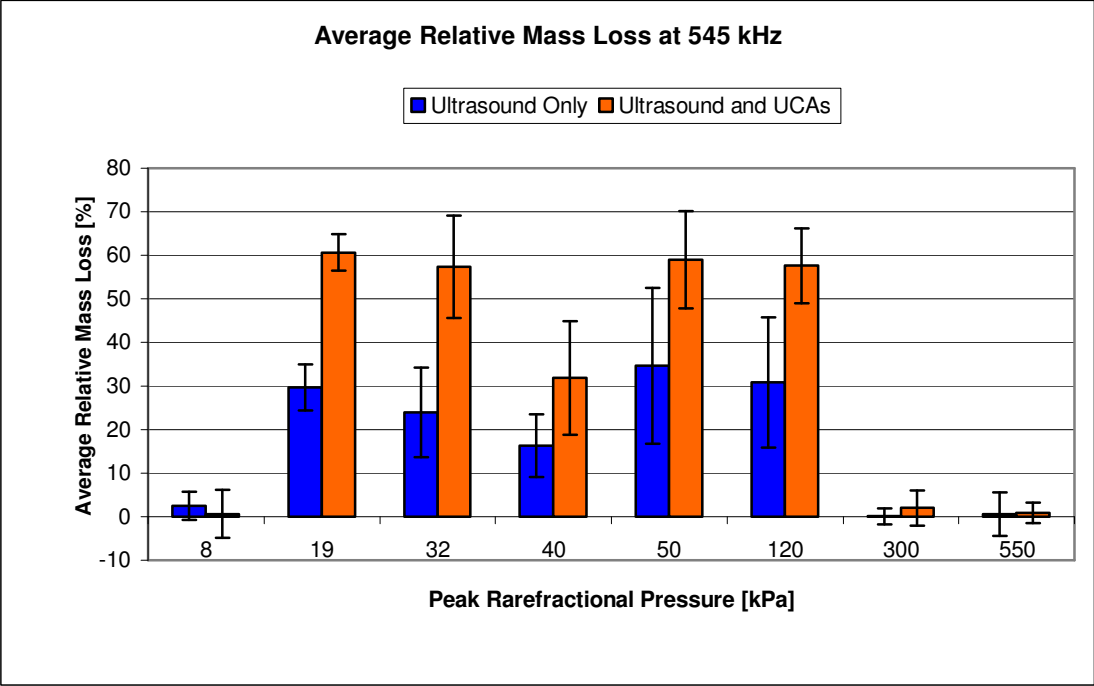


Figure 8.2. Average relative mass loss at a frequency of 545 kHz.

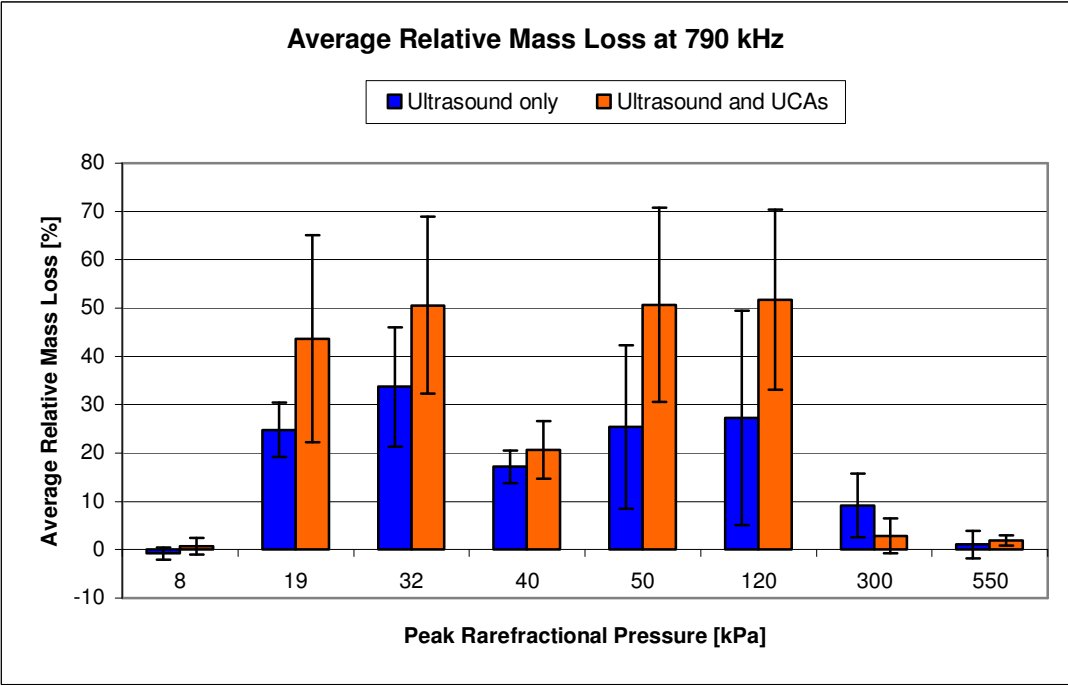


Figure 8.3. Average relative mass loss at a frequency of 790 kHz.

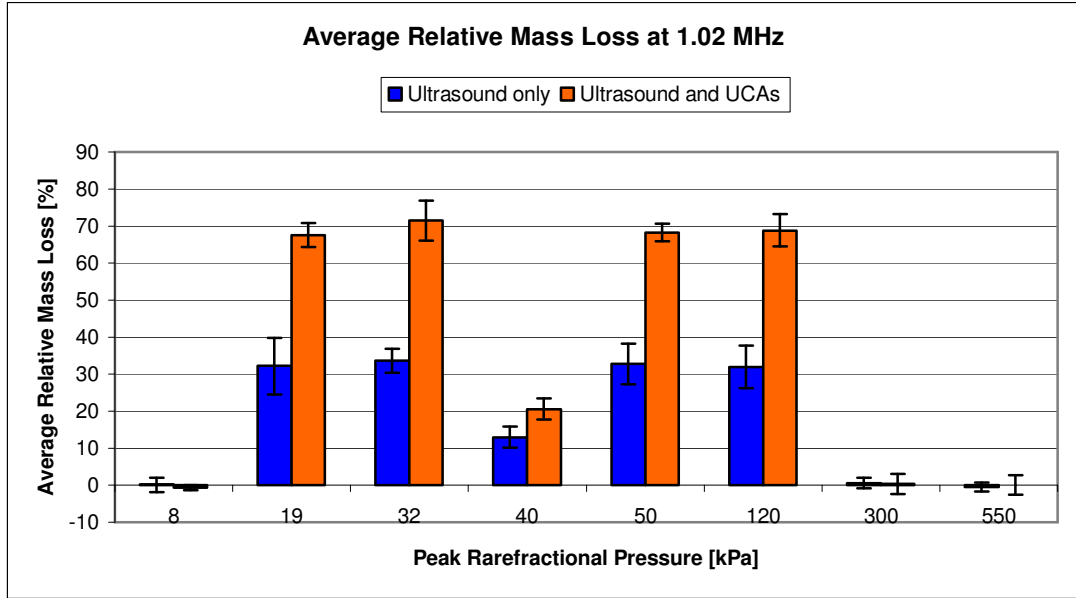


Figure 8.4. Average relative mass loss at a frequency of 1.02 MHz.

8.2.1 Analysis of Pressure Dependence of Average Relative Mass Loss

Figures 8.1 through 8.4 show that at a pressure of 8 kPa, for all frequencies, there is no significant difference in the average relative mass losses between samples exposed to ultrasound alone, $\overline{M}_{r(US)}$, (left bars in blue bars), and samples exposed to ultrasound when a contrast agent is present, $\overline{M}_{r(US+UCA)}$ (right bars in orange).

For all frequencies, pressures of 19, 40, and 120 kPa show significant differences in average relative mass losses between samples exposed to ultrasound only, $\overline{M}_{r(US)}$, and samples exposed to ultrasound with contrast agent, $\overline{M}_{r(US+UCA)}$. Samples exposed to ultrasound and Definity contrast agent lost significantly more mass than did samples exposed to ultrasound only.

At an exposure frequency of 395 kHz, pressures of 32 and 50 kPa did not have significant differences in average relative mass losses between samples exposed to ultrasound only, $\overline{M}_{r(US)}$, and ultrasound with contrast agent, $\overline{M}_{r(US+UCA)}$.

For all frequencies, exposure pressures of 300 and 550 kPa did not show significant differences in the average relative mass losses between samples exposed to ultrasound, $\overline{M}_{r(US)}$, and samples exposed to ultrasound and Definity® contrast agent, $\overline{M}_{r(US+UCA)}$.

In experimentation, it was observed that exposure to peak pressures of 300 and 550 kPa turned the sample bags containing the Definity contrast agent from opaque white to clear white. Exposure to peak pressures of 19, 32, 40, 50, and 120 kPa did not turn the sample bags containing Definity clear; those bags remained opaque white throughout the experiment.

8.3 Average Relative Mass Loss for Varying Frequencies

Figures 8.5 through 8.12 show the average relative mass losses, $\overline{M}_{r(US)}$ (Equation 7.8), and $\overline{M}_{r(US+UCA)}$ (Equation 7.9), for peak rarefractional pressures of 8, 19, 32, 40, 50, 120, 300, and 550 kPa with respect to center frequency. The sample size, $n = 6$, is consistent for each frequency, and the frequencies are represented in kilohertz.

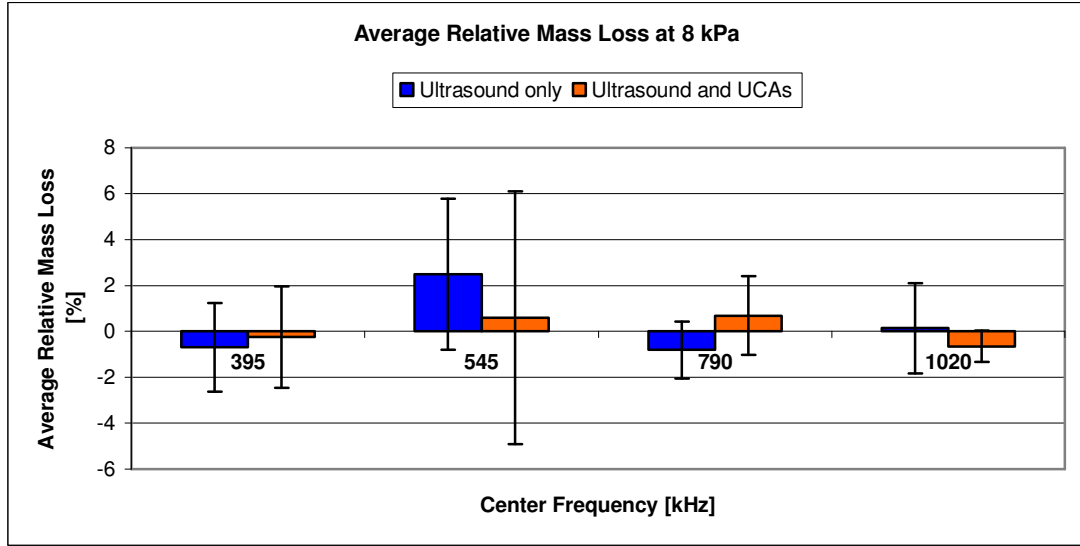


Figure 8.5. Average relative mass loss at a peak rarefractional pressure of 8 kPa.

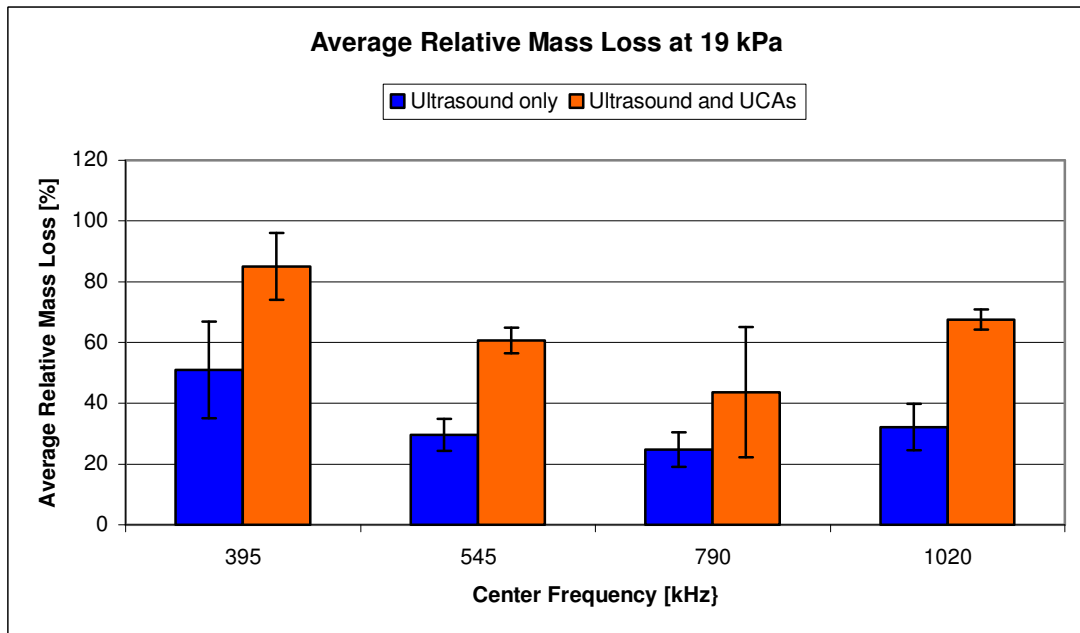


Figure 8.6. Average relative mass loss at a peak rarefractional pressure of 19 kPa.

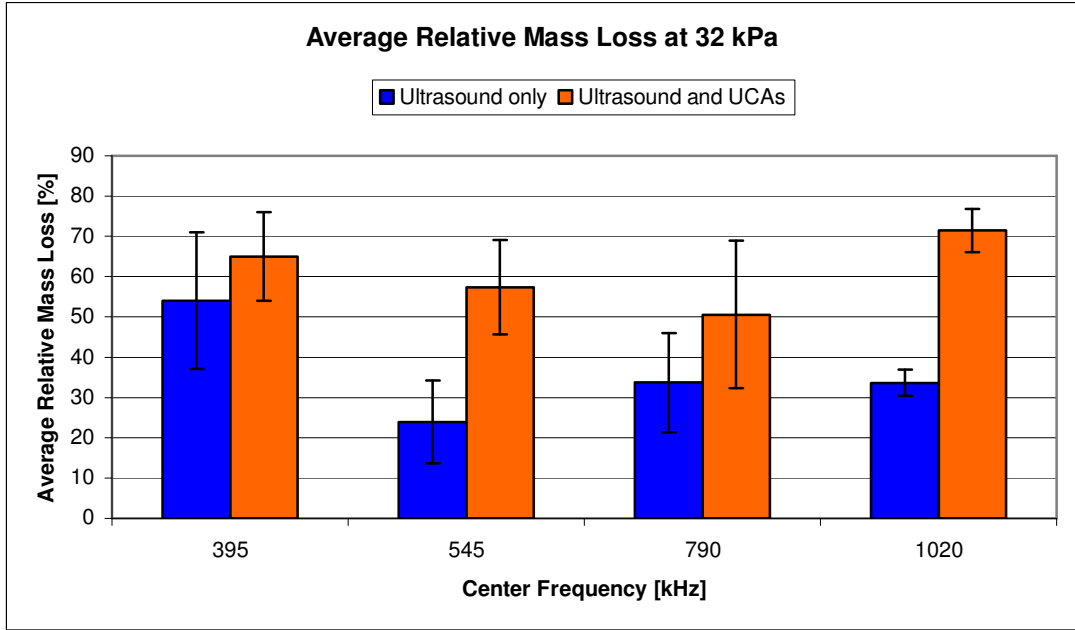


Figure 8.7. Average relative mass loss at a peak rarefractional pressure of 32 kPa.

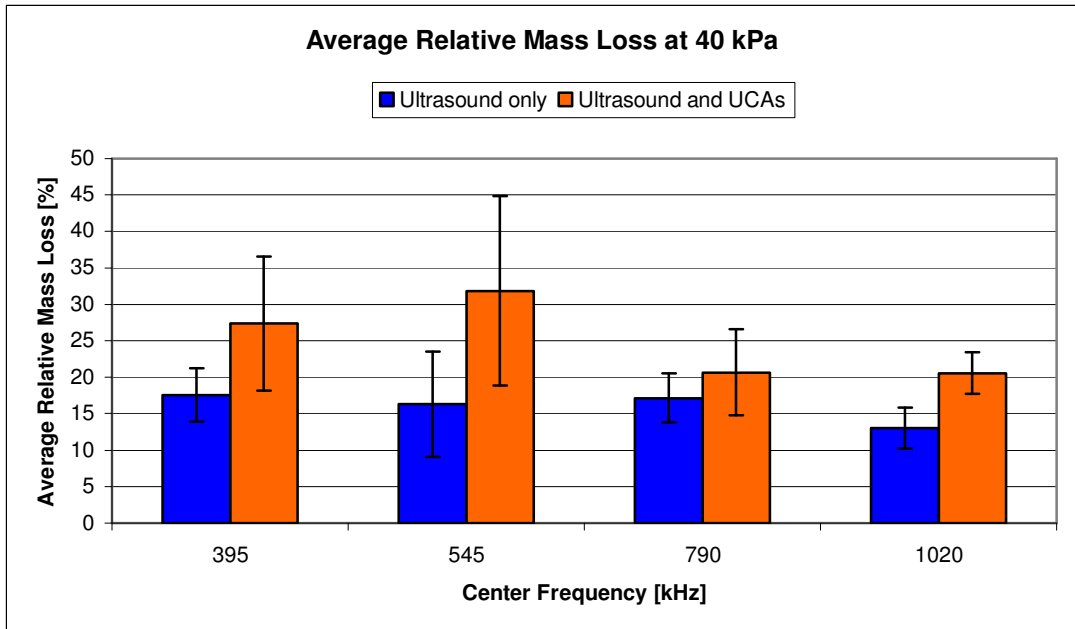


Figure 8.8. Average relative mass loss at a peak rarefractional pressure of 40 kPa.

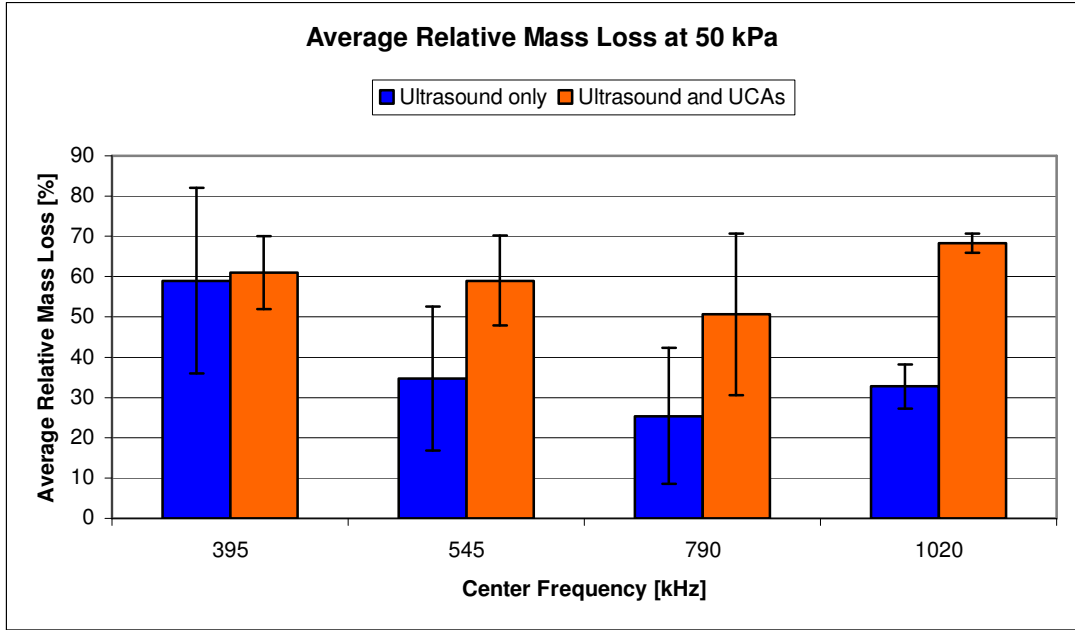


Figure 8.9. Average relative mass loss at a peak rarefractional pressure of 50 kPa.

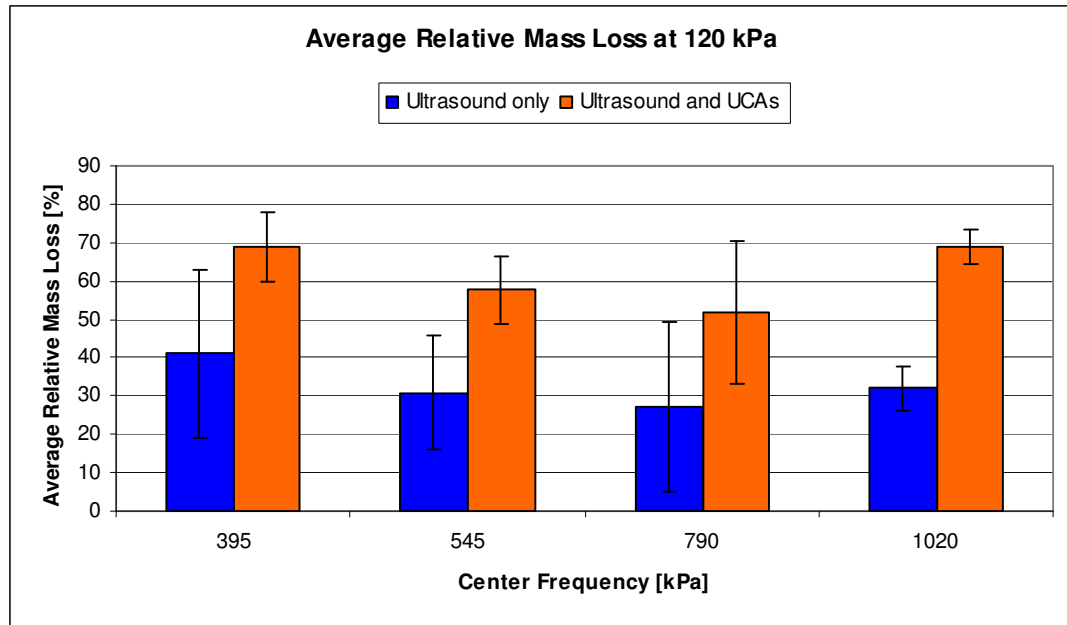


Figure 8.10. Average relative mass loss at a peak rarefractional pressure of 120 kPa.

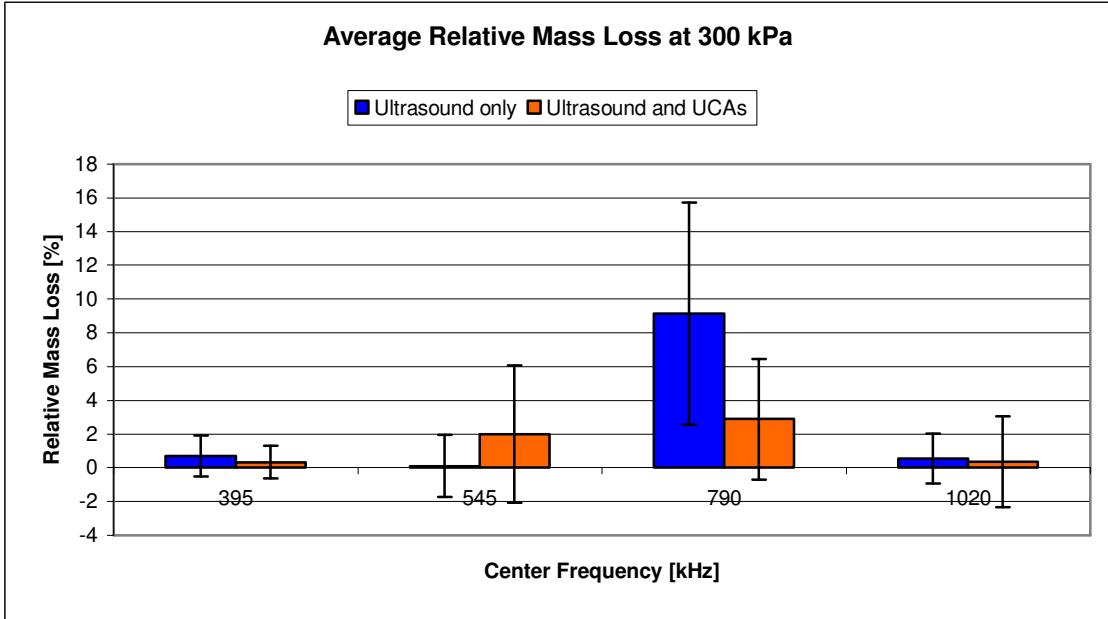


Figure 8.11. Average relative mass loss at a peak rarefractional pressure of 300 kPa.

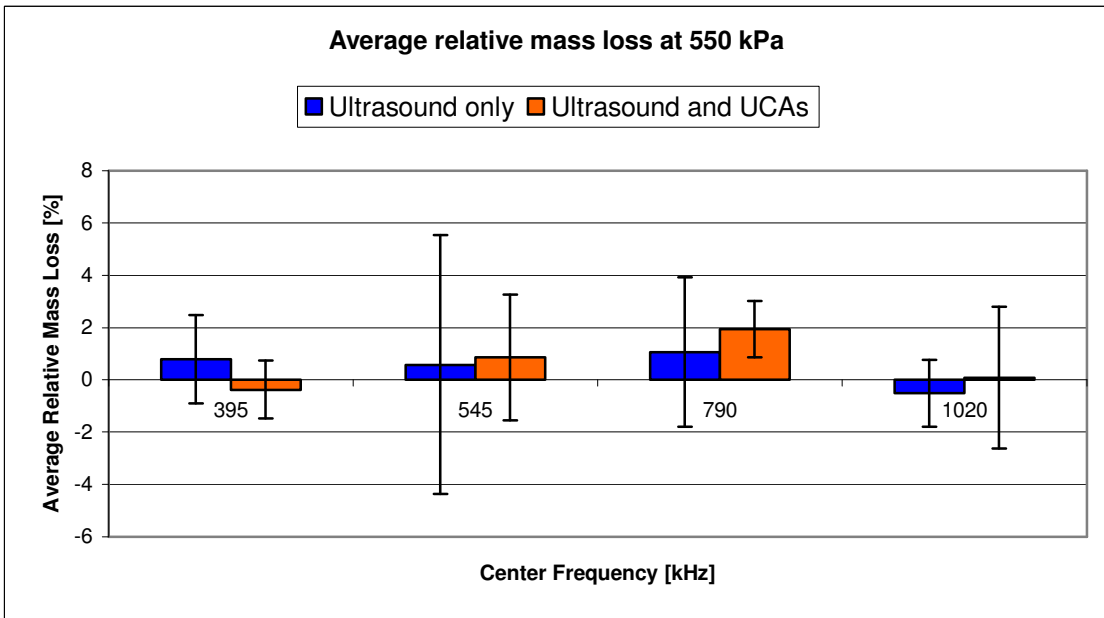


Figure 8.12. Average relative mass loss at a peak rarefractional pressure of 550 kPa.

8.3.1 Analysis of Average Relative Mass Loss for Varying Frequencies

Four exposure frequencies were used to examine frequency dependence, 395 kHz, 545 kHz, 790 kHz, and 1.02 MHz. Figures 8.5 through 8.12 show the average relative mass losses, $\overline{M}_{r(US)}$ (Equation 7.8), and $\overline{M}_{r(US+UCA)}$ (Equation 7.9), with respect to exposure frequency. At a peak rarefactional pressure of 8 kPa, there is no statistical significance in average relative mass losses between samples exposed to ultrasound only and samples exposed to ultrasound and contrast agent for all frequencies.

For a peak rarefactional pressure of 19 kPa (Figure 8.6), there is a statistical significance in the average relative mass loss between samples exposed to ultrasound only and samples exposed to ultrasound and contrast agent. There is also a significant decrease in amplitude of the average relative mass losses for samples exposed to ultrasound and samples exposed to ultrasound and contrast agent as frequency increases from 395 to 545 kHz. There is no significant change in the average relative mass loss between frequencies of 545 and 790 kHz, but there is a significant increase in amplitude of average relative mass loss between frequencies of 790 kHz and 1.02 MHz.

Figures 8.8 through 8.10 show that the trend in average relative mass loss with respect to frequency can no longer be statistically distinguished as decreasing or increasing with respect to frequency. The observed trend of decreasing average relative mass loss between frequencies of 395 and 545 kHz dissipates for pressures greater than 19 kPa. However, Figures 8.6, 8.7, 8.9, and 8.10 show that at a frequency of 1.02 MHz, the average relative mass loss for samples exposed to ultrasound and contrast agent is significantly greater than other exposure frequencies examined.

8.4 Bubble Displacement Amplitude and Oscillatory Viscous Shear Stress

Table 8.5 lists the simulated bubble displacement amplitudes, ξ , reported in micrometers; as a function of pressure, reported in Pascal; and frequency, reported hertz, found by solving the Marmottant equation, Equation 7.10, in MATLAB. Table 8.6 lists the calculated oscillatory viscous shear stress, S_c associated with the bubble displacement amplitude, in Pascal, calculated by Equation 7.13.

Bubble Displacement Amplitude, ξ (μm)

Pressure (kPa)	395 kHz	545 kHz	790 kHz	1.02 MHz
8	0.048	0.058	0.070	0.077
19	0.106	0.131	0.151	0.170
32	0.168	0.208	0.229	0.265
40	0.208	0.252	0.273	0.322
50	0.255	0.290	0.331	0.366
120	0.506	0.540	0.641	0.663
300	0.904	0.964	1.080	1.086
550	1.309	1.370	1.470	1.513

Table 8.5. Bubble displacement amplitudes, in microns, as a function of pressure and frequency.

Oscillatory Viscous Shear Stress, S_c (Pa)

Pressure (kPa)	395 kHz	545 kHz	790 kHz	1.02 MHz
8	133.07	261.44	544.41	887.51
19	292.81	585.95	1182.70	1948.90
32	465.33	932.85	1786.00	3036.70
40	573.70	1129.44	2136.70	3700.00
50	704.60	1296.09	2586.00	4189.40
120	1397.00	2418.38	5000.00	7603.60
300	2496.52	4315.60	8430.00	12446.00
550	3615.17	6172.10	11530.00	17342.00

Table 8.6. Oscillatory viscous shear stress, in Pascal, as a function of pressure and frequency.

8.5 Average Relative Mass Loss with Respect to Bubble Displacement Amplitude

Figures 8.13 through 8.16 show the average relative mass losses (Equations 7.8 and 7.9), in percentages, for simulated bubble displacement amplitudes, reported in micrometers, as shown in Table 8.5, for frequencies of 395 kHz, 545 kHz, 790 kHz, and 1.02 MHz.

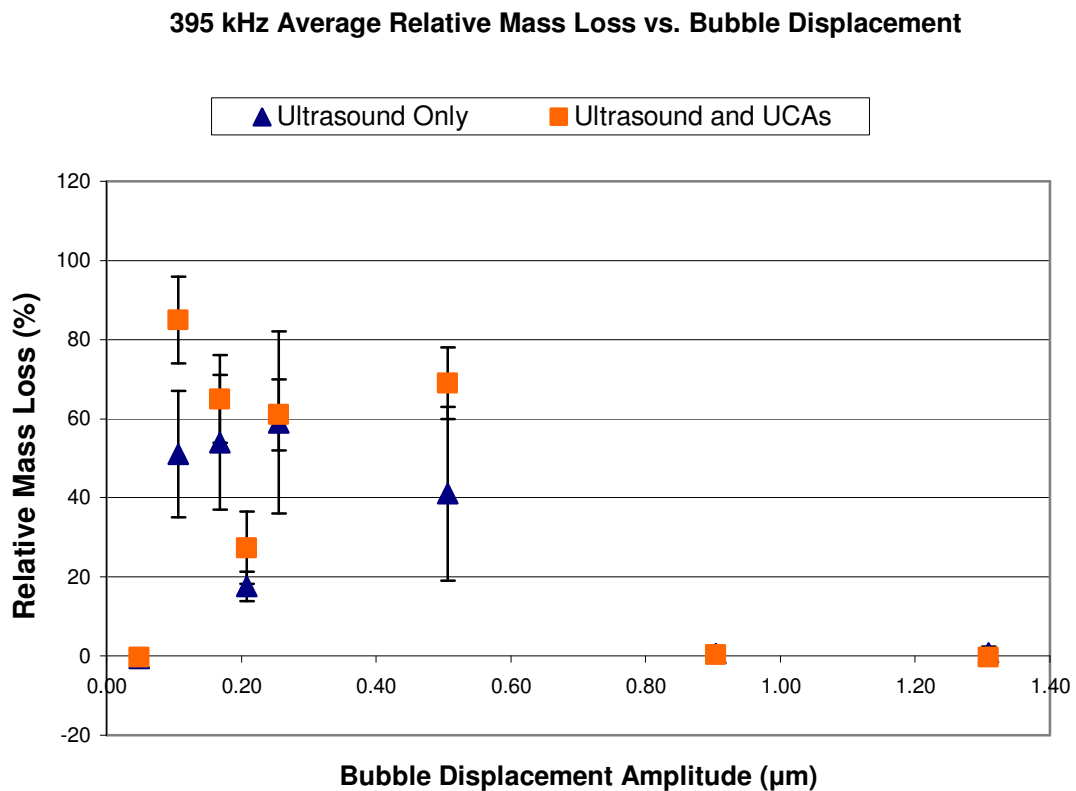


Figure 8.13. Average Relative mass loss with respect to simulated bubble displacement for 395 kHz.

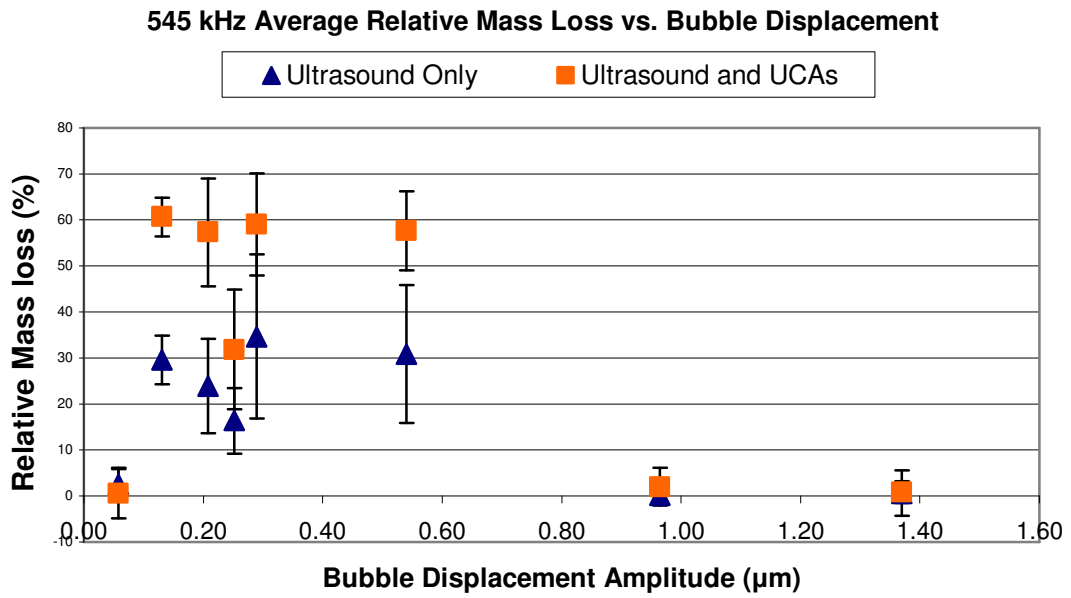


Figure 8.14. Average relative mass loss with respect to simulated bubble displacement at 545 kHz.

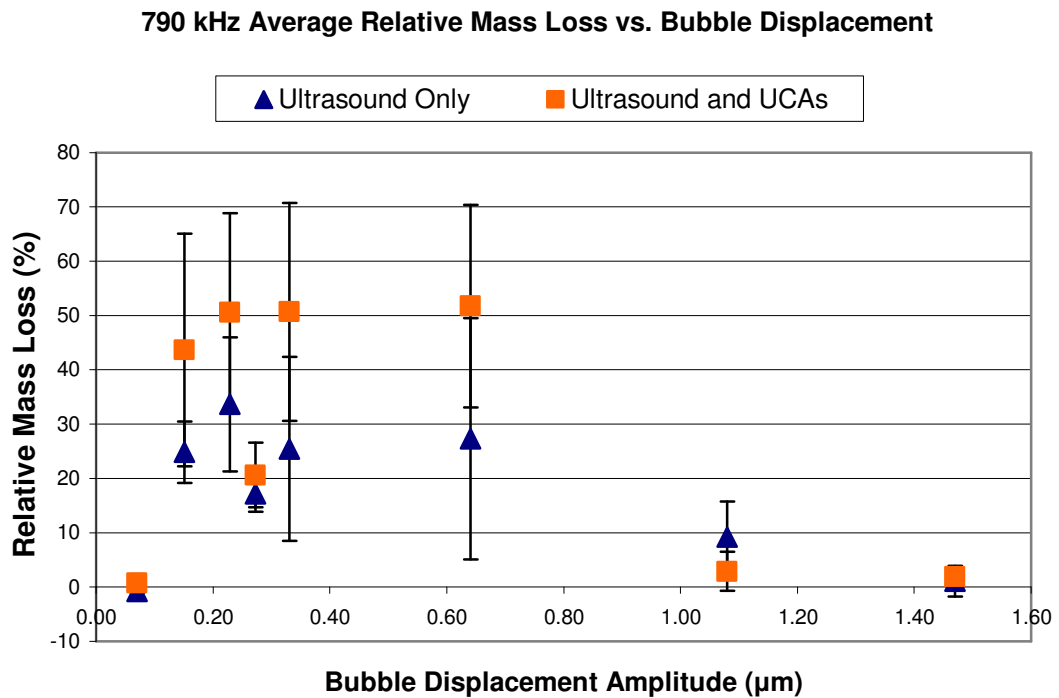


Figure 8.15. Average relative mass loss with respect to simulated bubble displacement at 790 kHz.

1.02 MHz Average Relative Mass Loss vs. Bubble Displacement

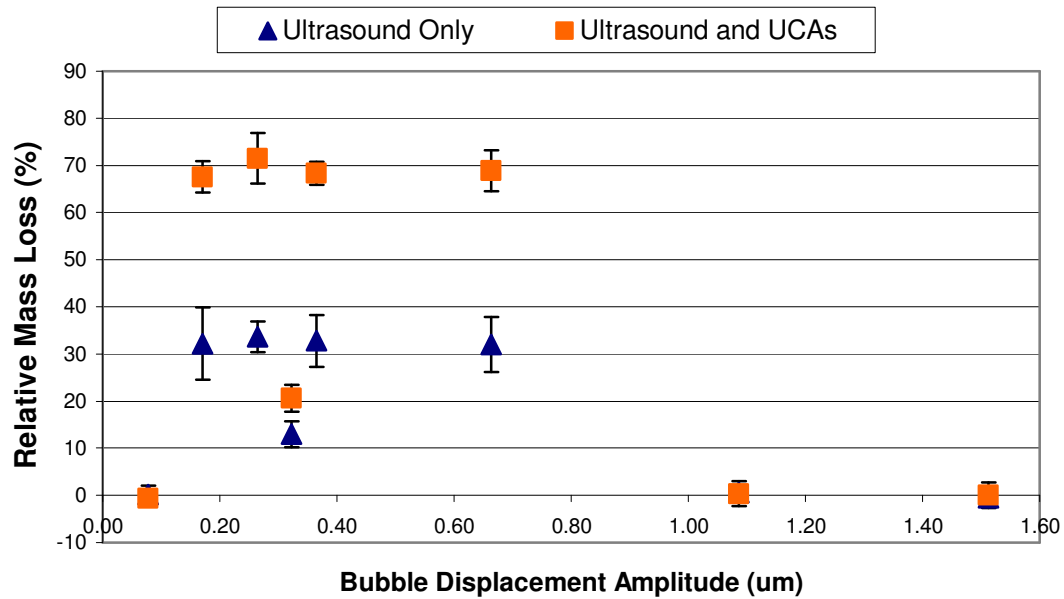


Figure 8.16. Average relative mass loss with respect to simulated bubble displacement at 1.02 MHz.

8.6 Frequency Dependence of Simulated Oscillatory Bubble Displacement on Average Relative Mass Loss

Figures 8.17 through 8.24 represent the average relative mass loss of samples exposed to 0.1 mL of Definity ultrasound contrast agent per 4 mL of degassed water only, $\overline{M}_{r(US+UCA)}$, calculated in Equation 7.9 and are plotted with respect to the simulated bubble displacement amplitudes derived by solving the Marmottant equations discussed in section 7.6. Each figure is fixed for a specific pressure and each data point represents a different exposure frequency, with the diamond representing 395 kHz, the square representing 545 kHz, the triangle representing 790 kHz, and the “x” representing 1.02 MHz. (The legend is provided in Figure 8.17 for reference. This legend applies to Figures 8.18 through 8.24 but is not shown.)

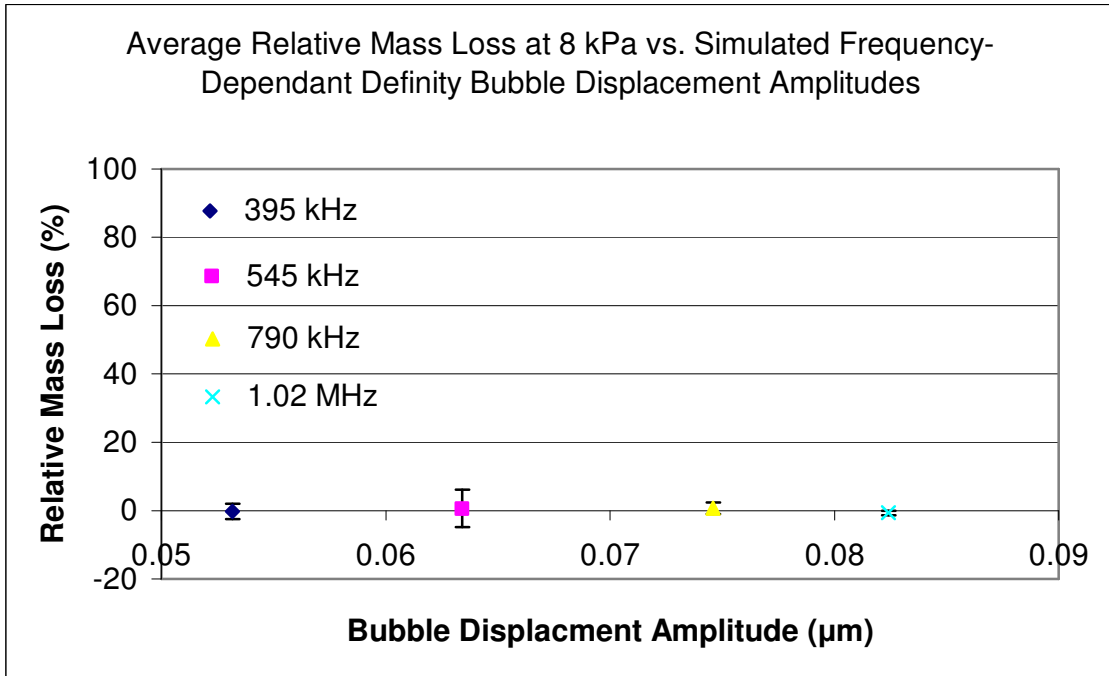


Figure 8.17. Average relative mass loss vs. simulated bubble displacement amplitudes with varying frequency at 8 kPa.

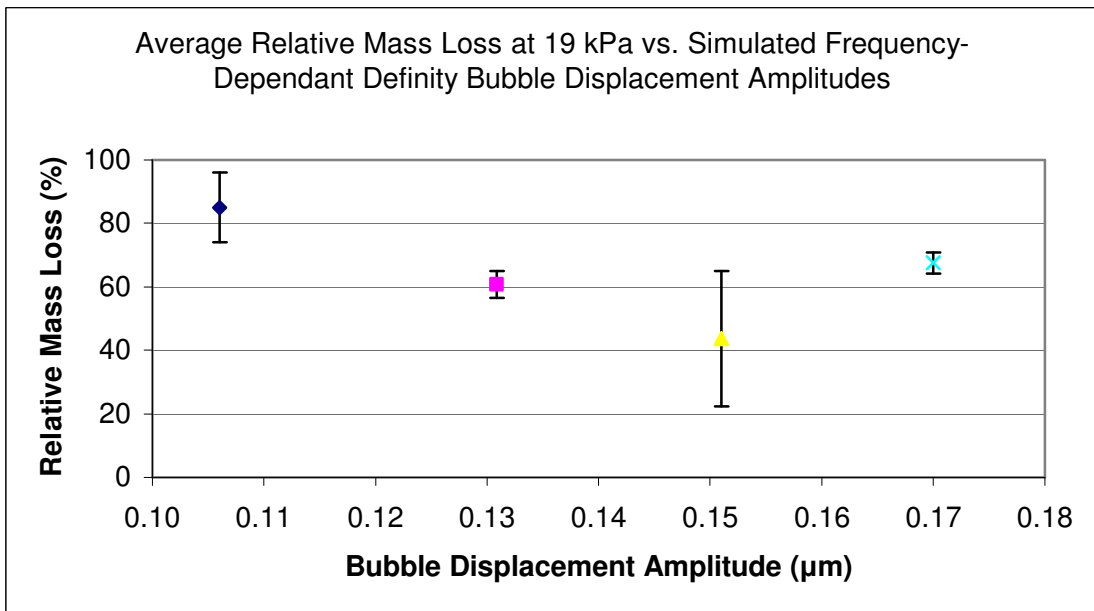


Figure 8.18. Average relative mass loss vs. simulated bubble displacement amplitudes with varying frequency at 19 kPa.

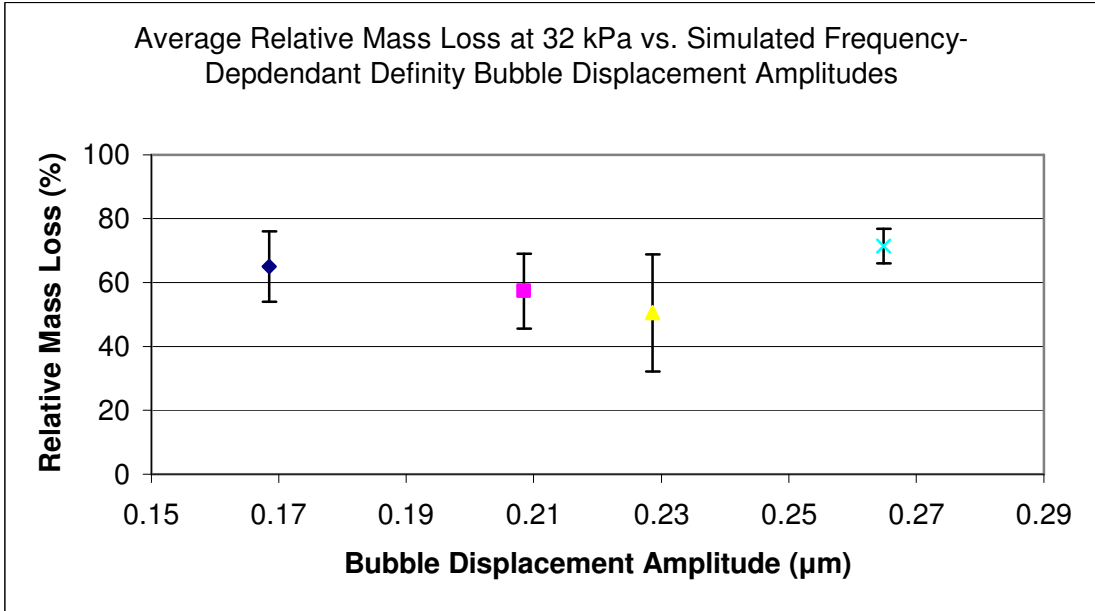


Figure 8.19. Average relative mass loss vs. simulated bubble displacement amplitudes with varying frequency at 32 kPa.

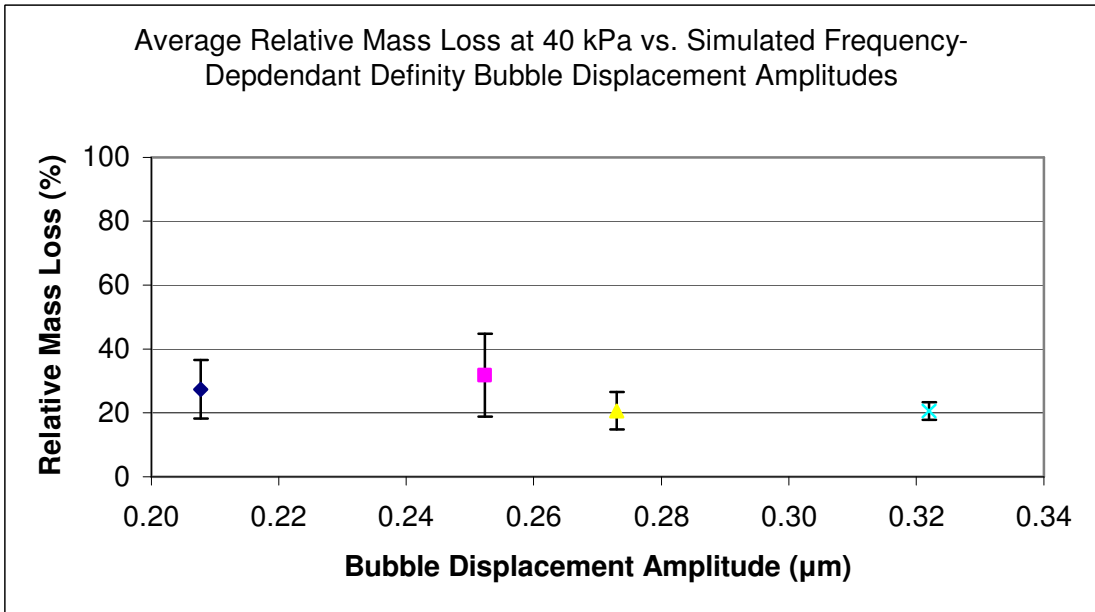


Figure 8.20. Average relative mass loss vs. simulated bubble displacement amplitudes with varying frequency at 40 kPa.

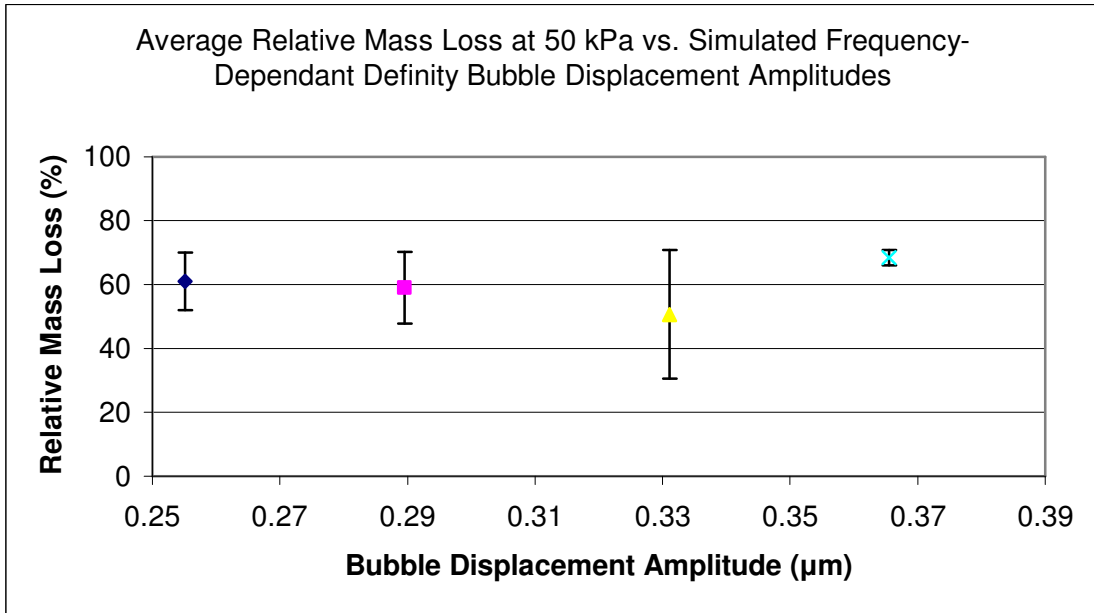


Figure 8.21. Average relative mass loss vs. simulated bubble displacement amplitudes with varying frequency at 50 kPa.

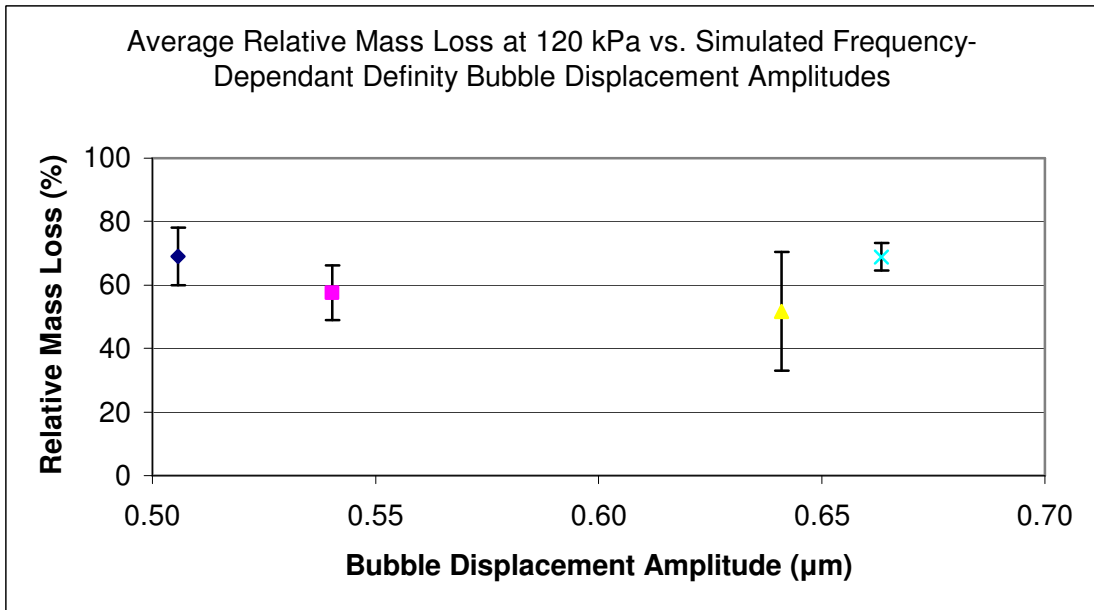


Figure 8.22 Average relative mass loss vs. simulated bubble displacement amplitudes with varying frequency at 120 kPa.

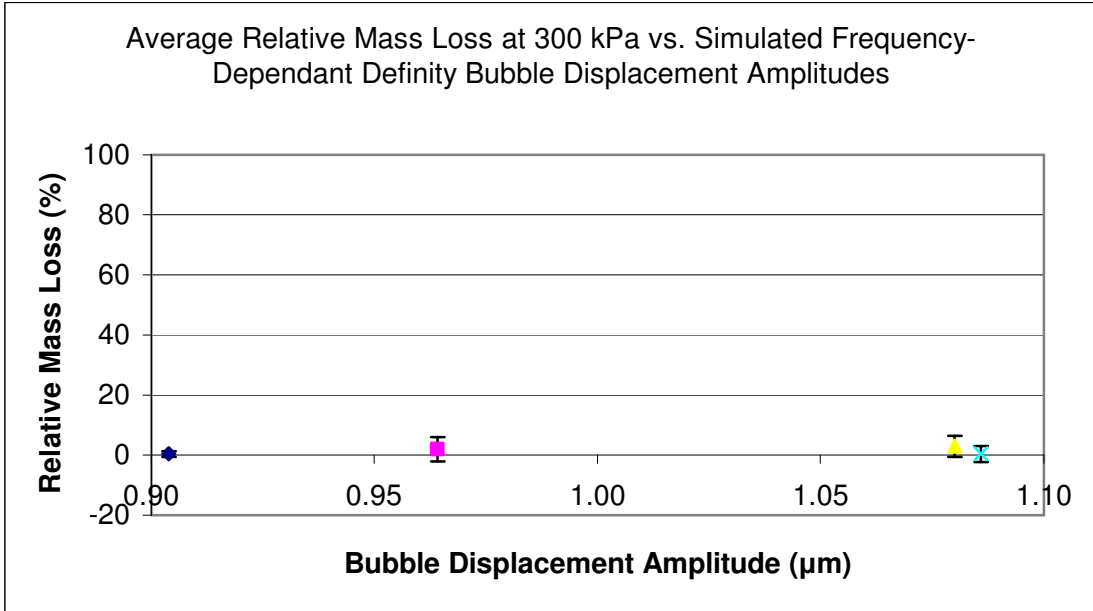


Figure 8.23. Average relative mass loss vs. simulated bubble displacement amplitudes with varying frequency at 300 kPa.

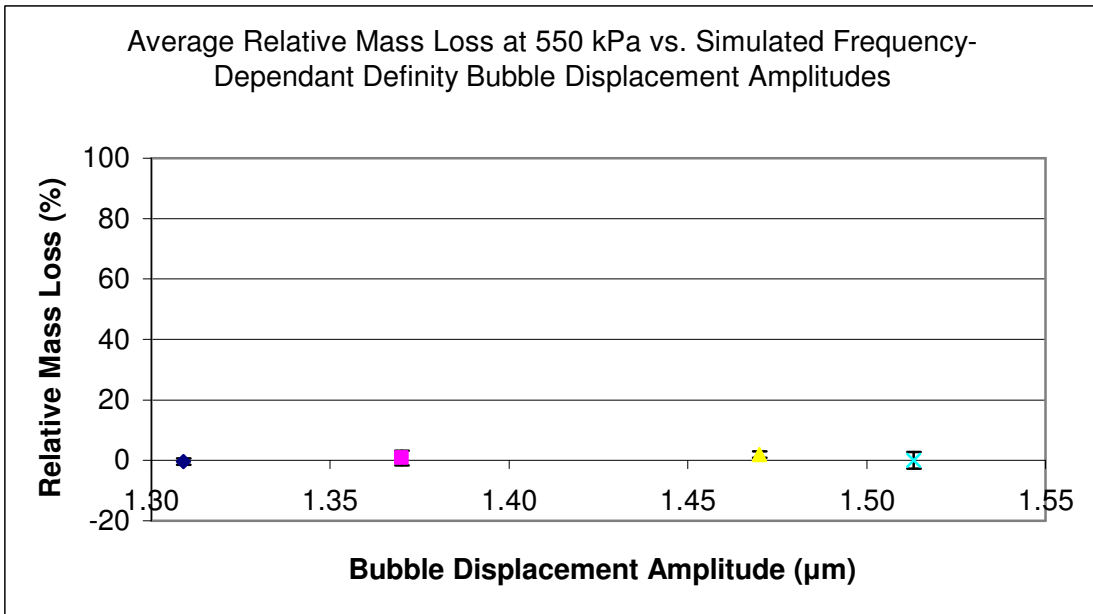


Figure 8.24. Average relative mass loss vs. simulated bubble displacement amplitudes with varying frequency at 550 kPa.

Chapter 9: Discussion

9.1 Displacement Amplitude, Shear Stresses, and Microstreaming

Stable cavitation of Definity contrast agent along with rt-PA has been shown to increase lysis in human blood clots at 120 kHz (Datta et al. 2008). Stable cavitation is a term used to describe the repeating oscillation of gas bodies that do not collapse. Acoustic pressures that induce stable cavitation are low in amplitude. However, if pressures are too low, stable cavitation will not occur (Husseini et al. 2005). As pressures increase, the cavitation becomes unstable, leading to inertial cavitation and the destruction of the gas body. It is known that oscillating gas bodies induce microstreaming. Lysis due to microstreaming is thought to correlate directly to the induced shear stresses that occur from nearby gas bodies oscillating close to a rigid structure (Williams et al. 1970; Rooney et al. 1972).

While examining the effects of shear stresses, it was reported that there is a threshold at which single gas body displacement amplitude, ξ , will cause cells to lyse. This effect was shown to saturate, however, as the bubble displacement amplitudes increased (Rooney et al. 1970). Figures 8.1 through 8.4 show the relative mass loss for exposure frequencies of 395 kHz, 545 kHz, 790 kHz, and 1.02 MHz for varying pressures, and Figures 8.13 through 8.16 show the average relative mass loss with corresponding simulated bubble displacement amplitudes, as calculated with Equation 7.10 and shown in Table 8.5.

At a pressure of 8 kPa, it is hypothesized that the threshold to cause lysis has not been reached; therefore, no significant mass loss occurs. This suggests that even though oscillating contrast agents are present, the oscillatory shear stresses, S_c , associated with

8 kPa for each frequency are not enough to induce any additional mass loss over controls.

As the pressure is increased, which increases the theoretical displacement amplitude of the bubbles, there is an increase in the associated oscillatory shear stress, S_c (Equation 7.13). As the oscillatory shear stresses increase, the relative mass losses are shown to increase significantly, indicating that under experimental conditions, the threshold to cause mass loss is between 8 and 19 kPa. Over theoretical bubble displacement amplitudes of 0.106 to 0.663 μm , or 19 to 120 kPa, respectively, this trend saturates and remains relatively invariable for all frequencies until a pressure of 300 kPa is reached. The saturation and invariability of the relative mass loss with increasing bubble displacement amplitude (Figures 8.13 through 8.16), support earlier findings and may indicate that oscillatory shear stresses are responsible for the induced mass losses seen (Rooney et al. 1970; Williams et al. 1970). At peak rarefractional pressures of 300 kPa and higher, it is hypothesized that a significant amount of the contrast agent has collapsed and is no longer present to oscillate and create any significant shear stresses in the vicinity of the clot. The lack of stable cavitation, or oscillating microbubbles, means there can be no increased cell lysis (Feril et al. 2004).

The invariability of the mass loss is also seen across frequencies. Figures 8.5 through 8.12 show fixed pressures with varying frequency. As the frequency is increased from peak rarefractional pressures of 19 to 120 kPa (Figure 8.6 through 8.10), the relative mass losses remain insignificant across each frequency, $P > 0.05$. Looking at relative mass loss as a function of the theoretical bubble displacement amplitudes (Figures 8.18 through 8.22), it appears that even though the bubble displacement

amplitudes increase as the source frequency increases, and thus the associated viscous shear stress increases, the relative mass loss seen is saturated. Increasing the frequency at these pressures does not increase the relative mass loss. Although constantly infused Definity contrast agent, under stable cavitation, has been shown to increase the thrombolysis of human blood clots, the response of clot lysis at multiple frequencies is not well understood (Datta et al. 2008). Frequency dependence as well as pressure dependence may give an overall picture of the mechanism involved.

While single-bubble oscillations were shown to induce hemolysis, an increased number of oscillating gas bodies increased the amount of lysis (Rooney et al. 1972). The amounts of lipid microspheres present in 0.1 mL of Definity contrast agent is approximately 1.2×10^9 bubbles. This quantity of oscillating contrast agent increased the amount of microstreaming and the associated shear stresses, which is hypothesized to cause the increase in average relative mass losses.

Figures 8.1 through 8.4 show that, for peak rarefactional pressures of 19 to 120 kPa, samples exposed to ultrasound and contrast agent have a significantly greater amount of average relative mass loss than samples exposed to ultrasound alone. At peak rarefactional pressures of 300 and 550 kPa, where a significant amount of contrast agent is hypothesized to have been destroyed, the lack of bubble activity and the associated lack of cavitation events correlate to lower mass loss. The lack of bubble activity supports the hypothesis that the presence of oscillating gas bodies, and thus associated microstreaming, is an important and necessary requirement for increases in relative mass loss.

It is hypothesized that peak rarefractional pressures of 19 to 120 kPa is not enough to collapse a significant amount of the contrast agent. Studies have shown that the single bubble collapse threshold for Definity at an exposure frequency of 0.91 MHz was reported at 1.4 MPa for a pulse duration of three cycles. Collapse threshold trends for Definity were shown to remain statistically invariable with increasing pulse duration but to increase with increasing frequency (Haak et al. 2007a, 2007b). The parameters of this study's exposure conditions were low frequencies (1.02 MHz and below), CW pulsing, and peak rarefractional pressures much less than 1.4 MPa. However, no certainty exists about the exact thresholds of Definity bubble cloud collapse thresholds at CW pulsing due to lack of research in this area.

As previously mentioned, peak rarefractional exposure pressures of 19 to 120 kPa did show an opaque bubble cloud throughout the exposure duration for samples exposed to ultrasound and Definity. The opaque white appearance indicates that bubbles are present in significant amounts (Definity 2008). The dissipation of the bubble cloud indicates that all bubbles within the beam have collapsed and are no longer present in significant amounts. Bubble cloud dissipation was seen for peak exposure pressures of 300 and 550 kPa.

An increase in relative mass loss for samples exposed to ultrasound alone for peak rarefractional pressures of 19, 32, 40, 50, and 120 kPa is hypothesized to occur by the ultrasonically induced formation and oscillation of gas bodies that result in stable cavitation and cause minor amounts of microstreaming (O'Brien et al. 2007). As previously mentioned, stable cavitation has been proposed as the main mechanism by which ultrasound enhances thrombolysis (Datta et al. 2008; Feril et al. 2004). The

addition of a contrast agent is hypothesized to increase stable cavitation events, and thus increase the amount of thrombolysis. Furthermore, samples exposed to ultrasound alone at 300 and 550 kPa did not show any increased relative mass loss over the matched controls, as it did for peak pressures of 19 to 120 kPa. The peak rarefactional pressure amplitudes were likely too great to sustain the induced gas bodies and collapsed any induced gas bodies much like it collapsed the Definity contrast agent (Husseini et al. 2005).

9.2 Resonance

Mass loss was seen to increase at a frequency of 1.02 MHz over 790 kHz consistently through all pressure values examined. An examination into the contrast agent used, Definity, showed that as the frequency increased to 1.02 MHz, the resonant frequency of the microbubble was being approached. The resonant frequency is the natural oscillating frequency. Definity has a reported resonant frequency between 1 and 4 MHz and correlates to a resonant frequency dependence of

$$\frac{3.25}{r}, \quad (9.1)$$

with r being the radius in micrometers (Chatterjee et al. 2005). When the resonant frequency is approached, the oscillations of the Definity contrast agent become maximized, increasing the amount of microstreaming activity, which is hypothesized to affect the overall relative mass loss. The size of the microbubbles affects the resonant frequency as well, with smaller bubbles resonating at higher frequencies than larger bubbles. Definity's published mean diameter ranges from 1.1 to 3.3 μm , which would put the resonant frequency between 2 and 6 MHz.

A contrast agent, such as Definity, also may resonate at ultraharmonics and subharmonics and may be responsible for increased lysis in human clots (Datta et al. 2008, Hussein et al. 2005). Ultraharmonics and subharmonics act as alternate resonant frequencies. It is hypothesized that subharmonic activity accounts for the average relative mass losses at all pressures being greater at a frequency of 395 kHz than at frequencies of 545 and 790 kHz. Figures 8.1 and 8.4 show that the average relative mass losses for samples exposed to ultrasound and contrast agent at frequencies of 395 kHz and 1.02 MHz, respectively, and peak rarefactional pressures of 19, 32, 40, 50, and 120 kPa are consistently and significantly greater than the average relative mass losses of samples under similar exposure conditions at frequencies of 545 and 790 kHz. At exposure frequencies of 395 kHz and 1.02 MHz, it is possible that the resonant oscillations of Definity create more microstreaming and therefore more average relative mass loss over non-resonant frequencies of 545 and 790 kHz. The average mass losses at a peak pressure of 19 kPa for frequencies of 1.02 MHz and 395 kHz (Figure 8.2) are not statistically significant, another indication that at resonant frequencies there is maximal microstreaming and thus maximal relative mass loss.

CHAPTER 10: CONCLUSIONS

Whole human blood clots were exposed to ultrasound only and ultrasound with Definity contrast agent, to test the hypothesis that oscillating microbubble activity, which causes microstreaming, is the main mechanism responsible for contrast agent-enhanced thrombolysis. Samples were exposed to continuous wave ultrasound at varying frequencies and pressures and then were compared to matched controls that were present in the same environment but did not undergo ultrasound exposure.

Frequency dependencies as well as pressure dependencies were examined to determine relative trends. Results were presented that show samples exposed to ultrasound and Definity contrast agent had significantly more mass loss than did samples exposed to ultrasound only.

Gas bodies believed to be oscillating at resonance or subharmonic frequencies were shown to be most efficient in thrombolysis enhancement, and the results agree with those of earlier studies (Datta et al. 2008; Hussein et al. 2005). Peak rarefactional pressures amplitudes, which were hypothesized to have collapsed a significant amount of contrast agent and therefore did not sustain oscillation activity, showed no increase in relative mass loss. Furthermore, low pressures and low frequencies were shown to be more likely to sustain stable cavitation.

REFERENCES

- Atar, Shaul, et al. "Using a Transducer-Tipped, High-Frequency Ultrasound Catheter and Local Low-dose Urokinase Delivery." *Journal of Endovascular Therapy* 8(2001): 282–290.
- Calliada, J., et al. "Ultrasound Contrast Agents: Basic Principles." *European Journal of Radiology* 27(1998): 157–160.
- Carmeliet, Peter, et al. "Inhibitory Role of Plasminogen Activator Inhibitor-1 in Arterial Wound Healing and Neointima Formation." *Circulation* 96(1997): 3180–3191.
- Carroll, R. C., et al. "Clot Retraction Facilitates Clot Lysis." *Blood* 57(1981): 44–48.
- Chatterjee, D., et al. "On the Suitability of Broadband Attenuation Measurement for Characterizing Contrast Microbubbles." *Ultrasound in Medicine and Biology* 6(2005):781–786.
- Cheng, Jason, et al. "In Vitro Microscopic Imaging of Enhanced Thrombolysis with 120-kHz Ultrasound in a Human Clot Model." *Acoustics Research Letters Online* 1(2005): 25–29.
- Cobbold, Richard. *Foundations of Biomedical Ultrasound*. New York: Oxford, 2007.
- Datta, Saurbha, et al. "Ultrasound-Enhanced Thrombolysis Using Definity® as a Cavitation Nucleation Agent." *Ultrasound in Medicine and Biology* 34(2008).
- Definity®. *Definity® Prescribing Information*. October 2007. Definity. 12 Feb 2008 <<http://www.definityimaging.com/pdf/prescribinginfo.pdf>>.

- Feril, Loreto, et al. "Biological Effects of Low Intensity Ultrasound: The Mechanism Involved, and Its Implications on Therapy and on Biosafety of Ultrasound." *Journal of Radiation Research* 45(2004): 479–489.
- Goertz DE, De Jong N, van der Steen AFW. "Attenuation and size distribution measurements of definity and manipulated definity populations". *Ultrasound in Medicine and Biology* 33(2007):1376-88.
- Haak, Alex, et al. "Detection of Microbubble Ultrasound Contrast Agent Destruction Applied to Definity[®]" *Proceedings of the International Congress on Ultrasound*, Paper Number 1719, 2007a.
- Haak, Alex, et al. "Semiautomatic Detection of Microbubble Ultrasound Contrast Agent Destruction Applied to Definity Using Support Vector Machines." *Proceedings of the IEEE Ultrasonics Symposium* 1(2007b): 660–663.
- Harmening, Denise. *Clinical Hematology and Fundamentals of Hemostasis*. 4th ed. Philadelphia: F.A. Davis, 2002.
- Hoff, Lars. *Acoustic Characterization of Contrast Agents for Medical Ultrasound Imaging*. Dordrecht, the Netherlands: Kluwer, 2001.
- Hojima, Y., et al. "In Vitro Activation of the Contract (Hageman Factor) System of Plasma by Heparin and Chondroitin Sulfate E." *Blood* 63(1984): 1453–1459.
- Holland, Christy, et al. "Ultrasound-enhanced Tissue Plasminogen Activator Thrombolysis in an In Vitro Porcine Clot Model." *Thrombosis Research* 121(2008): 663–673.
- Husseini, Ghaleb A., et al. "The Role of Cavitation in Acoustically Activated Drug Delivery." *Journal of Control Release* 107(2005): 253–261.

- Kinsler, Lawrence, et al. *Fundamentals of Acoustics*. 4th ed. New York: Wiley, 2000.
- Kline, JA, et al. “Emergency Clinician-Performed Compression Ultrasonography for Deep Venous Thrombosis of the Lower Extremity.” *Annals of Emergency Medicine*: Jun 16 (2008) [Epub ahead of print].
- Langévin, P. French Patent No. 505,703 (filed September 17, 1917; Issued August 5, 1920).
- Levi, Marcel, et al. “Bidirectional Relation Between Inflammation and Coagulation.” *Circulation* 109(2004): 2968–2704.
- Magnus, E. Ohman, et al. “Intravenous Thrombolysis in Acute Myocardial Infarction.” *Chest* 119(2001): 253S–277S.
- Marmottant, P., et al. “A Model for Large Amplitude Oscillations of Coated Bubbles Accounting for Buckling and Rupture.” *Journal of the Acoustical Society of America* 118(2005): 3499–505.
- Meunier, Jason M., et al. “Duty Cycle Dependence of Ultrasound Enhanced Thrombolysis in a Human Clot Model.” *Ultrasound in Medicine & Biology* 4(2007): 576–583.
- National Council on Radiation Protection and Measurements (NCRP). *Exposure Criteria for Medical Diagnostic Ultrasound: II. Criteria Based on All Known Mechanisms. Recommendations of the National Council on Radiation Protection and Measurements*. NCRP Report No.140. Bethesda, MD: NCRP, 2002. 574 pp.
- Newton, I. *Philosophiae Naturalis Principia Mathematica*. Cambridge: Royal Society London, 1687.

- Nyborg, Wesley L., et al. "Biophysical Implications of Bubble Dynamics." *Applied Scientific Research* 38(1982):17–24.
- O'Brien, William. "Ultrasound-Biophysics Mechanisms." *Biophysics & Molecular Biology* 93(2007): 212–255.
- Prokop, Adrian, et al. "Cavitation Mechanisms in Ultrasound-Accelerated Fibrinolysis." *Ultrasound in Medicine & Biology* 33(2007): 924–933.
- Rayleigh, J. W. S. *The Theory of Sound*. New York: Dover, 1945.
- Rooney, J. A., et al. "Hemolysis Near an Ultrasonically Pulsating Gas Bubble." *Science* 169(1970): 869–871.
- Rooney, James A., et al. "Shear as a Mechanism for Sonically Induced Biological Effects." *Journal of the Acoustical Society of America* 52(1972): 1718–1724.
- Rosenschein, Uri, et al. "Analysis of Coronary Ultrasound Thrombolysis Endpoints in Acute Myocardial Infarction (ACUTE Trial)." *Circulation* 95(1997): 1411–1416.
- Rosenschein, U., et al. "Coronary Ultrasound Thrombolysis: From Acute Myocardial Infarction to Saphenous Vein Grafts and Beyond." *Current Interventional Cardiology Reports* 3(2001): 5–9.
- Stocum, David. *Regenerative Biology and Medicine*. Burlington, MA: Elsevier Academic Press, 2006.
- Stone, Michael, et al. "Pulsed-high intensity focused ultrasound enhanced t-PA mediated thrombolysis in a novel in vivo clot model, a pilot study." *Thrombosis Research* 121(2007): 193–202.

- Stroke rt-PA, Stroke Study Group. "Tissue Plasminogen Activator for Acute Ischemic Stroke." *The New England Journal of Medicine* 333(1995): 1581–1588.
- Suchkova, V. N., et al. "Effect of 40-kHz Ultrasound on Acute Thrombotic Ischemia in a Rabbit Femoral Artery Thrombosis Model: Enhancement of Thrombolysis and Improvement in Capillary Muscle Perfusion." *American Heart Association* 101(2000): 2296–2301.
- Szabo, Thomas. *Diagnostic Ultrasound Imaging*. Burlington, MA: Elsevier Academic Press, 2004.
- Tachibana, Katsuro, et al. "Albumin Microbubble Echo-Contrast Material as an Enhancer for Ultrasound Accelerated Thrombolysis." *Circulation* 92(1995): 1148–1150.
- Williams, A. R., et al. "Hemolysis Near a Transversely Oscillating Wire." *Science* 169(1970): 871–873.
- Williams, A. R., et al. Possible Alteration in the Permeability of Ascites Cell Membranes after Exposure to Acoustic Microstreaming." *Journal of Cell Science* 12(1973): 875–885.
- Yano, Yuichiro, et al. "Determinants of Thrombin Generation, Fibrinolytic Activity, and Endothelial Dysfunction in Patients on Dual Antiplatelet therapy: Involvement of Factors Other Than Platelet Aggregability in Virchow's Triad." *European Heart Journal* 29(2008): 1729–1738.
- Zimbaro, G. "Contrast Agent Ultrasonography (Voiding Urosonography) of Vesicoureteral Reflux: State of the Art." *Radiology in Medicine* 112(2007): 1211–1224.

APPENDIX A

Figures I.1 through I.4 show calibration curves for 395 kHz, 545 kHz, 790 kHz, and 1.02 MHz. Pressures are plotted with respect to function generator voltage in millivolts.

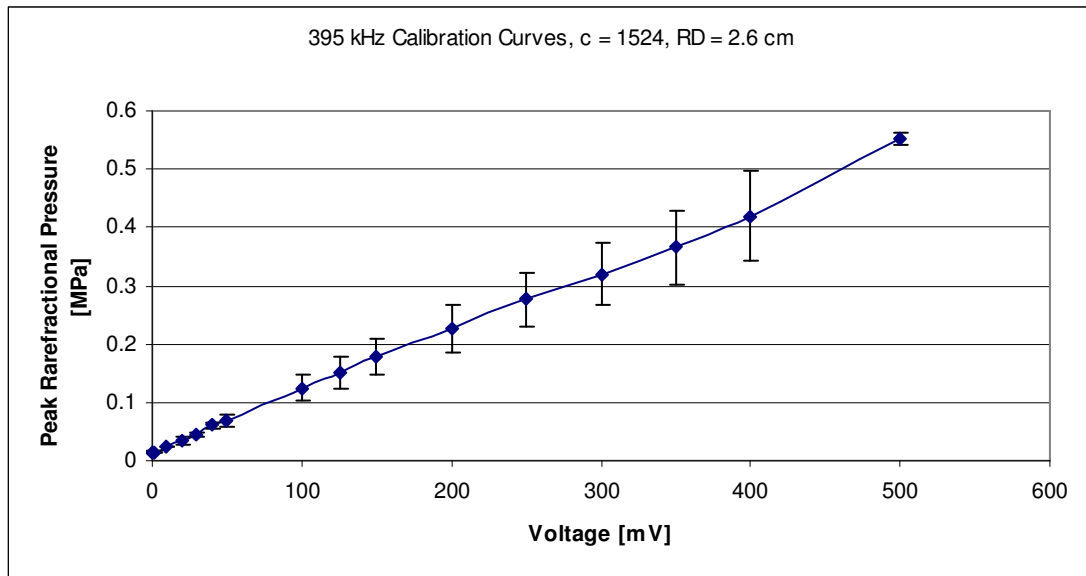


Figure A.1. Calibration curve for 395 kHz.

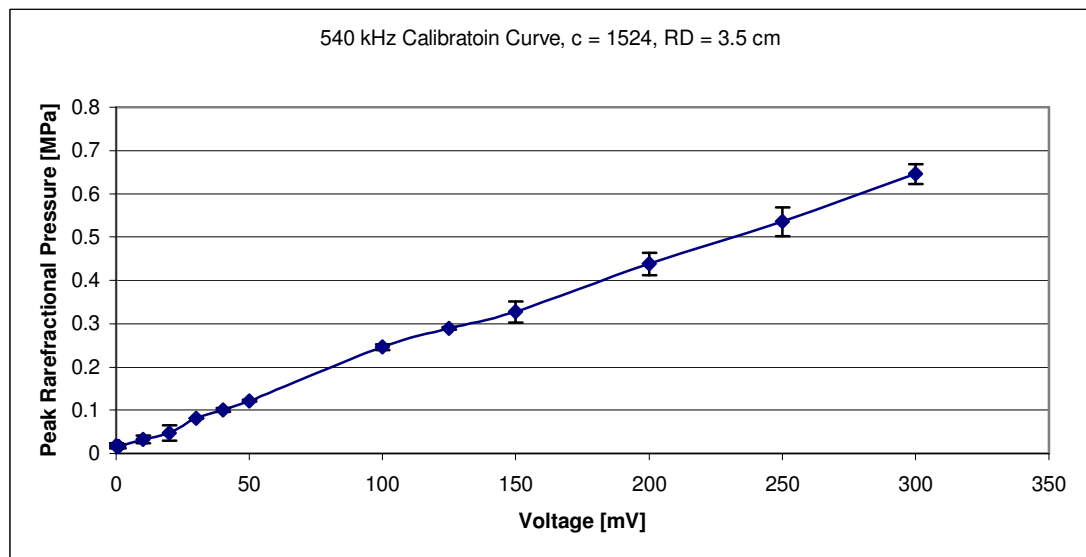


Figure A.2. Calibration curve for 545 kHz.

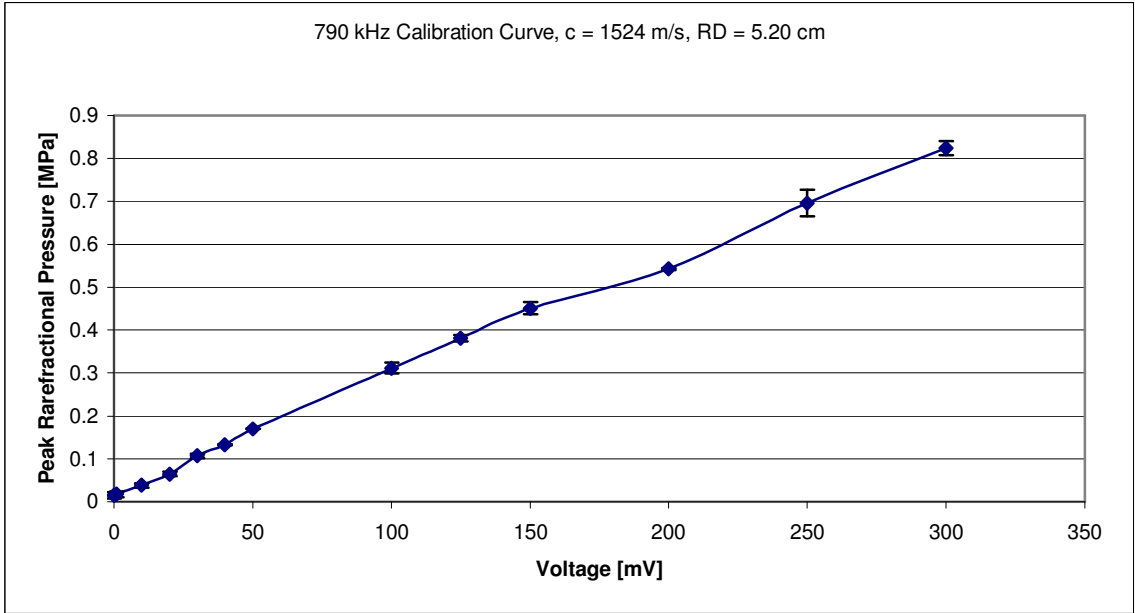


Figure A.3. Calibration curve for 790 kHz.

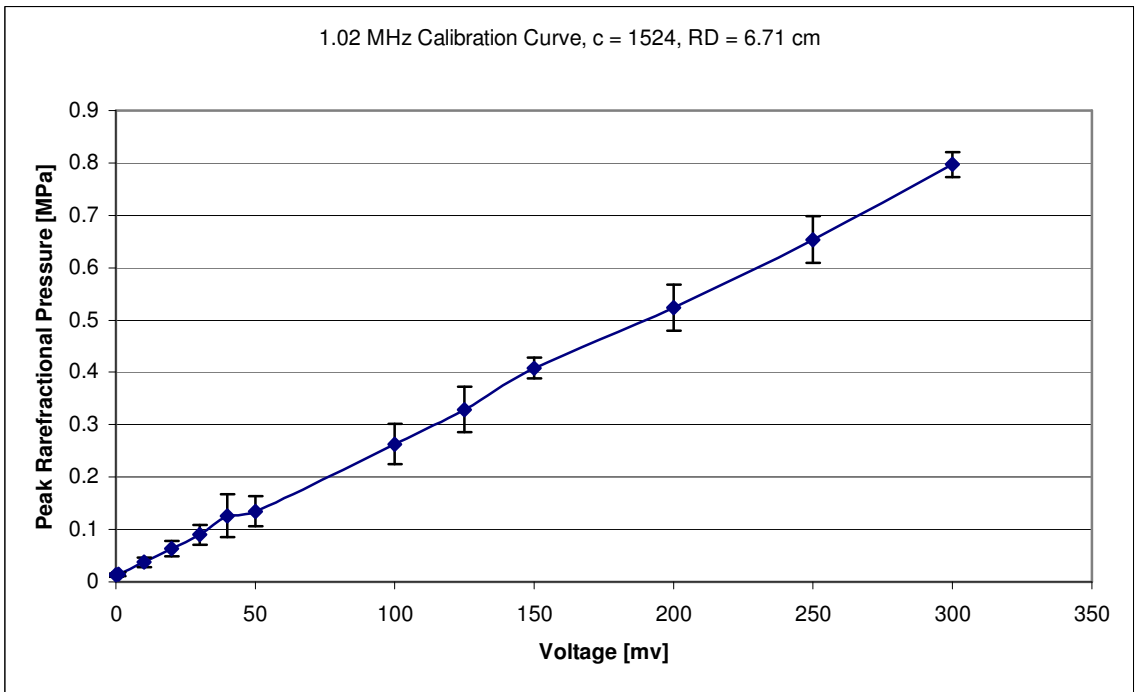


Figure A.4. Calibration curve for 1.02 MHz.

APPENDIX B

Figures II.1 through II.4 are -6dB beamwidth plots for 395 kHz, 545 kHz, 790 kHz, and 1.02 MHz.

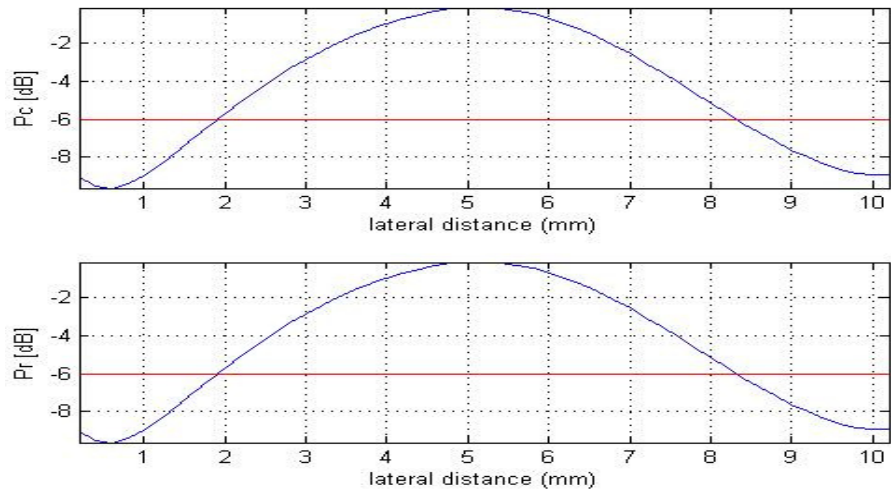


Figure B.1. 395 kHz, -6dB beamwidth.

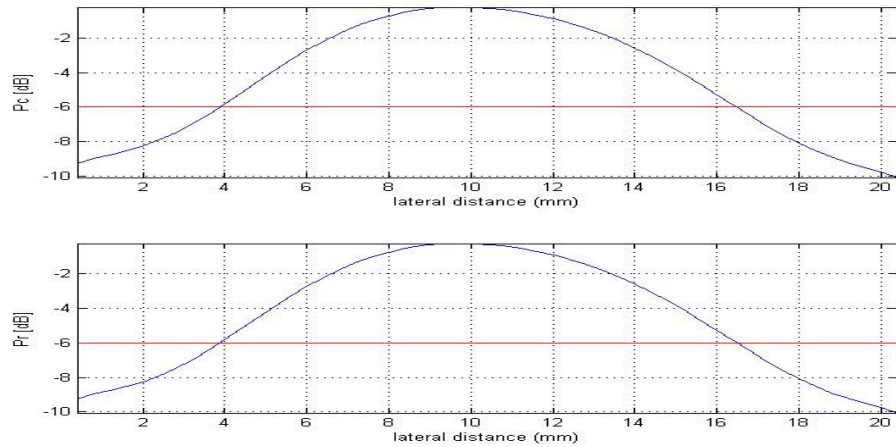


Figure B.2. 545 kHz, -6dB beamwidth.

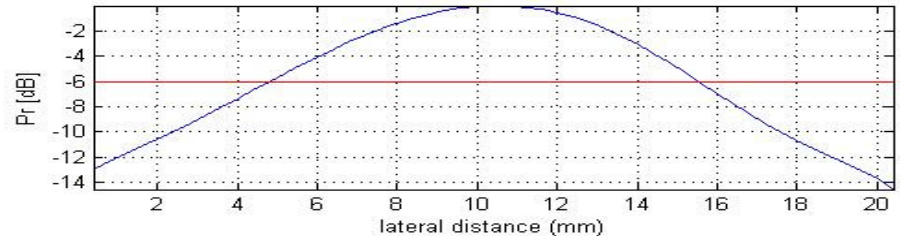
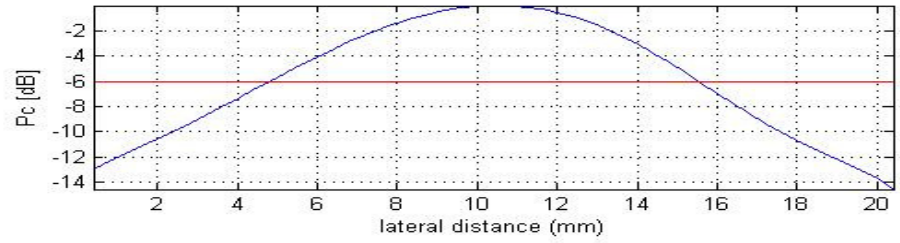


Figure B.3. 790 kHz, -6dB beamwidth.

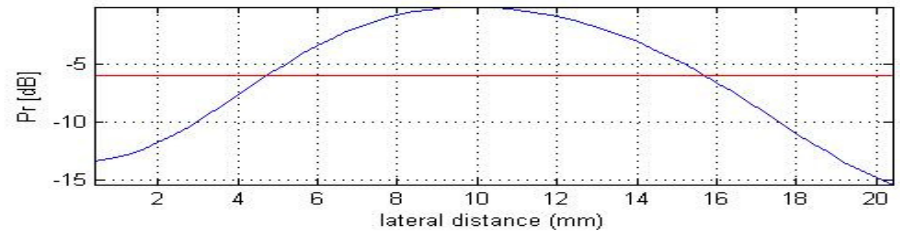
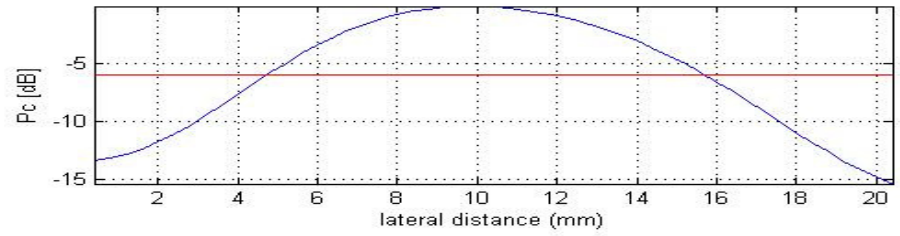


Figure B.4. 1.02 MHz, -6dB beamwidth.